The feasibility of EM navigation for gynecologic brachytherapy catheter insertion

Lisanne Venix

Surgery, Antoni van Leeuwenhoek Hospital
University of Twente
2023

UNIVERSITY OF TWENTE.

NETHERLANDS CANCER INSTITUTE
ANTONI VAN LEEUWENHOEK

Lisanne Venix

Master Thesis

Chairman Medical Supervisor	**Prof. dr. T.J.M. Ruers** NKI – Antoni van Leeuwenhoek Hospital Department of Surgical Oncology
Medical Supervisor	**Dr. F.J. Siepel** University of Twente Faculty of Electrical Engineering, Mathematics and Computer Science
Daily Supervisor Technical Supervisor	**Dr. W.J. Heerink** NKI – Antoni van Leeuwenhoek Hospital Department of Surgical Oncology
Professional Behavior Supervisor	**Drs. J. de Witte** University of Twente Faculty of Science and Technology
External member	**MSc. J.R. Abbing** University of Twente Faculty of Electrical Engineering, Mathematics and Computer Science

September 1, 2023

Lisanne Venix
The feasibility of EM navigation for gynecologic brachytherapy catheter insertion

University of Twente, Technical Medicine, Faculty of Science and Technology
Netherlands Cancer Institute, Antoni van Leeuwenhoek Hospital, Surgical oncology

Master Thesis
September 1, 2023

Abstract

Introduction Accurately inserting catheters for gynecologic brachytherapy (GBT) can be difficult and time-consuming, especially for complex GBT procedures involving placement of one or more freehand catheters next to the applicator, through the perineal or vaginal tissue. Electromagnetic (EM) tracking for real-time visualization during catheter placement might improve catheter placement accuracy and procedure time. This study aims to develop and evaluate an EM-navigation system for 3D assistance during GBT catheter insertion.

Method A new EM-navigation workflow was proposed, involving EM-tracked transrectal ultrasound, an in-house developed catheter insertion stylet, and dedicated software. The accuracy of the EM system, the US calibration, and the EM-tracked insertion stylet was measured. Phantom tests were conducted to assess initial accuracy and system usability. Additionally, a case study was conducted with 'regular' GBT procedures to test the first part of the proposed workflow in a clinical setting. The accuracy of gold marker (GM) localization, registration techniques, and overlay discrepancies were examined.

Results The average EM-system accuracy was 0.64 mm, and the average jitter was 0.02. The transverse US calibration had a fiducial registration error (FRE) of 1.47 mm and a target registration error (TRE) of 1.59 mm. The sagittal US calibration had an FRE of 0.67 mm and a TRE of 0.72 mm. The calibration RMS of the EM-tracked stylet was 0.23 mm and the mean position error was 0.54 mm. For the phantom tests, the mean FRE was 0.83 mm for the initial registration and 0.74 mm for the tumor tracker registration. The mean overall US-catheter to EM-catheter distance was 1.69 mm. The mean US-catheter tip to EM-catheter tip distance was 3.04 mm. During the clinical cases, a mean FRE of 2.4 mm was acquired for both the MRI-US registration and the CT-US registration. Besides, the inserted catheters were tracked with an inter-catheter geometry accuracy of 3.4 mm.

Conclusion This study showed that EM-navigation for gynecological brachytherapy catheter insertion is feasible in a research setting and has potential in a clinical setting. The proposed workflow has potential benefits that eliminate the need for intraoperative CBCT. This workflow can only truly be analyzed after the prospective clinical study in our institution.

Keywords *- Electromagnetic tracking; Gynecological Brachytherapy; Ultrasound; Freehand catheters*

Acknowledgements

In October 2022, I started my 'TG-schap' at the surgical department of the Netherlands Cancer Institute, Antoni van Leeuwenhoek Hospital. During the past year, I gained clinical experience in the surgical, gynecologic, and radiotherapy departments, and I wrote this master's thesis, to finish the master's program of Technical Medicine with the track Medical Imaging and Interventions at the University of Twente.

I would like to thank all my supervisors, with a special thanks to my daily supervisor Wout Heerink, for always thinking along and being enthusiastic about the project. I also want to thank the radiation oncologists that were involved, with special thanks to Eva Rijkmans and Eva Schaake, for providing clinical insights and guidance. Besides, I want to thank the clinical implementation team at the OR, and all the colleagues at The Vide for all the help and the nice coffee and lunch breaks. Lastly, a big thank you to my friends and family, who always support and motivate me.

I look back with great pleasure on my time at the Image Guided Surgery group at the AvL and I am looking forward to starting my journey as a PhD student at this department.

Lisanne Venix
2023

Contents

List of Figures

List of Tables

List of Abbreviations

2D	Two-dimensional
3D	Three-dimensional
5DOF	Five degrees of freedom
6DOF	Six degrees of freedom
BT	Brachytherapy
CTV	Clinical target volume
CBCT	Cone-beam computed tomography
CPI	Clinical Physics and Informatics (Dutch: KFI)
CT	Computed tomography
DSMH	Decontamination, Sterilization, and Medical Devices Hygiene
EBRT	External beam radiation therapy
EM	Electromagnetic
EMTS	Electromagnetic tracking system
FG	Field-generator
FRE	Fiducial registration error
GBT	Gynecologic brachytherapy
GM	Gold marker
HDR	High-dose-rate
IMDD	Investigational Medical Device Dossier
LACC	Locally advanced cervical cancer
LDR	Low-dose-rate
MDR	Medical Devices Regulation
MERC	Medical Ethics Review Committee (Dutch: METC)
MRI	Magnetic Resonance Imaging
OAR	Organ at risk
OR	Operation room
RMS	Root Mean Square
RTO	Radiation oncologist
SCU	System Control Unit
SIU	Sensor Interface Unit
TRE	Target registration error
TRUS	Transrectal ultrasound
US	Ultrasound

1 Introduction

1.1 Clinical background

1.1.1 Gynecological anatomy

The female pelvic organs and structures include the urinary bladder and urethra, the rectum and anus, and the female reproductive system, including the uterus, the cervix, the vagina, the ovaries, and the fallopian tubes (Fig. 1). The uterus is a pear-shaped organ, consisting of the fundus, body, and cervix, positioned between the urinary bladder (anterior) and the rectum (posterior) (Fig. 1, Fig. 2). The uterus is naturally anteverted and anteflexed, meaning that the fundus is located more anteriorly than the cervix so that the cervix forms an angle between the body and vagina and the mass of the uterus lies over the bladder [1, 2]. The position of the uterus and the cervix are dependent on bladder and rectum filling. The variations in position differ per person but the angle of anteversion and angle of anteflexion (Fig. 2) are generally larger when the bladder is filled because the bladder pushes the uterine body more superiorly and more posteriorly. The cervix and the vagina are pushed anteriorly when the rectum is filled. [3]

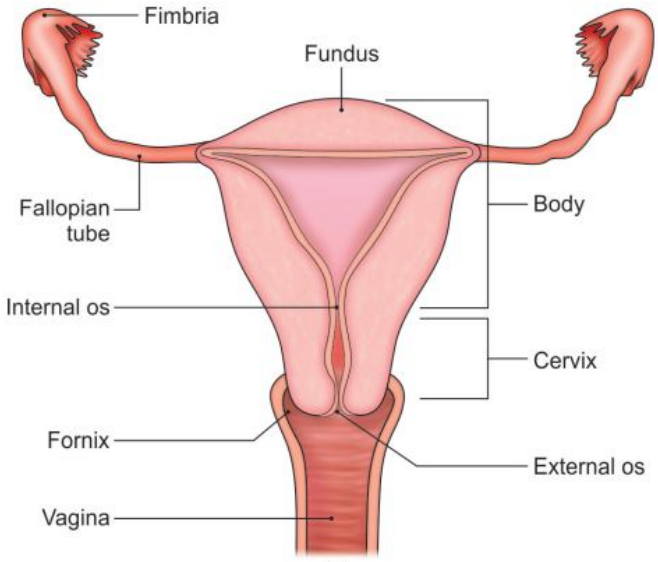

Figure 1. Anterior view of the uterus [4].

1.1.2 Gynecological malignancies

Gynecological malignancies are all malignancies in the female reproductive system, including cervical, ovarian, uterine, vaginal, vulvar, and fallopian tube cancer. Surgery, external beam radiotherapy (EBRT), and chemotherapy are considered options for these types of cancers. For uterine, vaginal, and cervical cancers, high-dose-rate (HDR) brachytherapy can be considered an additional treatment modality. [5]

1.1.3 Brachytherapy

Brachytherapy (BT), literally meaning 'short-therapy', is a radiation technique where radioactive seeds or sources are placed very close to or inside the tumor, being able to deliver a high dose to the tumor while minimizing the dose to the organs at risk [5, 6]. For high-dose-rate (HDR) BT, or pulsed-dose-rate (PDR) BT, which are used for uterine, vaginal and cervical cancers, radioactive sources are sent through an inserted applicator,

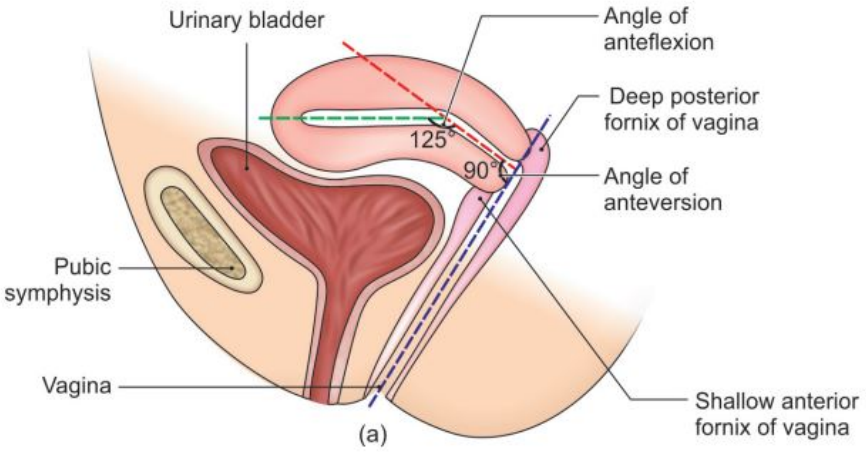

Figure 2. Angulations of the uterus and vagina [4].

with or without additional catheters. HDR BT is mainly indicated for patients with locally advanced cervical cancer after a period of chemoradiation and for patients with surgically treated uterine endometrial cancer for decreasing the risk of vaginal vault recurrence or in case of vaginal recurrence after radical hysterectomy. For locally advanced cervical cancer (LACC), the 5-year disease-free survival rate was 76.7% for patients receiving concomitant chemoradiation plus BT, against 69.3% for patients receiving neoadjuvant chemotherapy plus surgery [5]. For endometrial cancer, the disease-free survival rate after surgery and BT is 82.7% [7].

LACC patients usually receive three or four fractions of BT in two to three applications. Applications are generally planned with an interval of one week. Intraoperatively and under general anesthesia, the radiation oncologist (RTO) places a BT applicator against the cervix with an intrauterine tube inside the uterus, enabling intracavitary BT. Besides, a specified number of interstitial catheters are inserted through the applicator, inside the cervix and tumor, guided by a preoperatively made plan based on magnetic resonance imaging (MRI) (Fig. 3). These catheters enable interstitial BT. In some complex cases, the clinical target volume (CTV) constraints are not met with only the intrauterine tube and the interstitial catheters placed through the applicator, wherefore the RTO places additional freehand catheters, transperineally or transvaginally. [6, 8, 9]

1.1.4 Image guidance during the standard freehand gynecological BT catheter insertion procedure

The standard gynecological BT (GBT) catheter insertion procedure is as follows: The tumor and surrounding organs at risk (OARs) are preoperatively segmented in the MRI. Ultrasound (US) and Cone-beam Computed Tomography (CBCT) are available intraoperative imaging modalities. The intrauterine tube of the applicator is placed inside the uterus with abdominal US guidance. The RTO palpates the catheter trajectory transvaginally, wherefore it is often easier to insert the catheters before placing the applicator. In some cases, the catheters are visualized with abdominal or transrectal US (TRUS). An intraoperative CBCT gives more detailed information, based on which catheters can be replaced if necessary. Postoperatively, an additional MRI is made which is used for planning the dose distribution. [6]

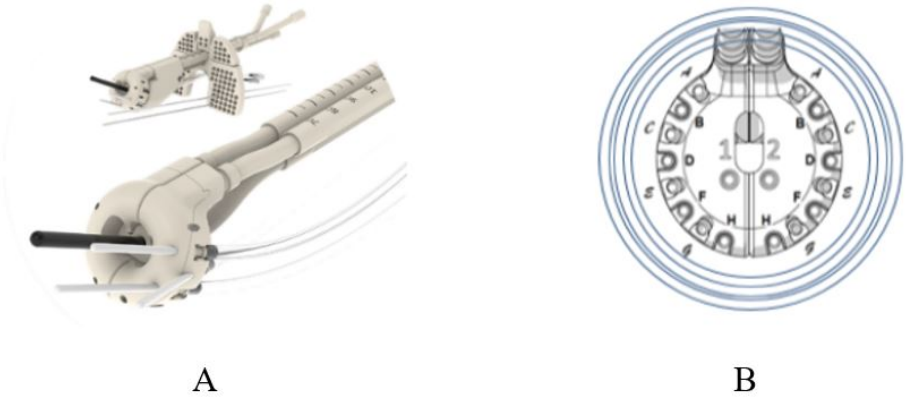

Figure 3. A) The Venezia Brachyterapy applicator [10] B) the template used for GBT catheter planning.

1.2 Technical background

1.2.1 Surgical navigation

Surgical navigation is a technology involving real-time tracking and visualization of surgical instruments and anatomical structures, providing detailed spatial information to the surgeon during the operation [11–15]. Surgical navigation is used for a wide range of applications, including needle placement, tumor resection, and orthopedic surgery. Surgical navigation requires (image) co-registration of the patient's preoperative data, such as CT or MRI scans, with the intraoperative situation, such as CBCT or US. To perform surgical navigation, specialized hardware and software are required, including tracking sensors, imaging devices, and a navigation system that processes and displays the gathered data in a user-friendly manner.

1.2.2 Electromagnetic tracking system

Electromagnetic tracking systems (EMTSs) consist of an EM field generator (FG), a System Control Unit (SCU), a Sensor Interface Unit (SIU), and EM sensors (Fig. 20). The FG emits a low-intensity, varying EM field, which induces a voltage in the coils inside the EM sensors positioned in the magnetic field. This voltage induction is measured by the SCI, which amplifies and digitizes the electric signals. The SCU processes and analyses the signal, determining the position and the orientation of the sensors.

Sensors are defined as 5 degrees of freedom (DOF) or 6DOF. Degrees of freedom describe the number of axes in which a change in position or rotation can be detected. With 5DOF sensors, the translation is reported in x-, y- and z- positions and two of the orientations are reported in yaw and pitch. 6DOF sensors also report a third orientation of the sensor, which is called the roll. [16–19]

With the use of (image) co-registration between the EM coordinate system and intraoperative imaging, and between intraoperative and preoperative imaging, the EM sensors can be visualized relative to the anatomical target. EM tracking is relatively fast, easy to use, and does not require a direct line of sight to the generator like optical tracking systems. The downsides of EM tracking are potential field distortions by ferromagnetic materials close to or inside the magnetic field, causing inaccurate measurements, as well as the inconvenience of wires that connect the sensors. [17, 20–23]

Figure 4. From left to right: an Aurora NDI FG, SCU, and SIU [17]

1.2.3 Image registration

Image registration is an imaging processing technique to align images acquired from different modalities or time points, and is a crucial component of surgical navigation systems. Mathematically, rigid image registration can be represented as finding a 4×4 transformation matrix, T, that optimally transforms a source image, I_s, to a target image, I_t. A common method for image registration is landmark-based registration, which aims to match anatomical landmarks in the source image, ${}^{Is}p$, to their corresponding landmarks in the target images, ${}^{It}p$. The corresponding landmarks in the two images can be correlated by [24]:

$$ {}^{It}p = {}^{It}_{Is}T\,{}^{Is}p \tag{1} $$

where ${}^{It}_{Is}T$ is the transformation matrix from the source image to the target image. This is a complex problem to solve, as ${}^{It}_{Is}T$ contains 7 degrees of freedom, which are 3 from the rotation matrix, 3 from the translation vector, and 1 from the scaling factor. However, as the dimensions of medical images often correspond (mm), scaling is usually not applied for medical image registration. In case of an optimal registration, the sum of squared error SE would be zero:

$$ SE = \sum_{n=1}^{N} ||{}^{It}p_n - {}^{It}_{Is}T\,{}^{Is}p_n||^2 = 0 \tag{2} $$

In reality, the registration will not be perfect, and the SE will be larger than 0. By solving this equation as an optimization problem where SE is minimal, ${}^{It}_{Is}T$ is found. Several approaches to finding the transformation matrix exist, all involving a method for data association, alignment, and error measurement.

Data association is the process to match each landmark ${}^{Is}p_n$ to their corresponding landmark ${}^{It}p_n$. There are some automatic approaches to obtain this association, which involve trial and error, iterative closest point, feature matching, and learning-based methods [24, 25]. The trial and error method uses all possible combinations and tries to align the points; the alignment with the lowest error is chosen as the final alignment. The iterative closest point algorithm calculates the Euclidean distance between ${}^{Is}p_n$ and ${}^{It}p_n$ and matches the closest

points. After alignment and error measurement, the data association is performed again until a minimal error is acquired. The feature-matching approach calculates a unique feature vector for each point and uses these features for association. Learning-based approaches have received attention in recent years. They are often more robust than classical methods and have great potential for a variety of tasks.

Data association is followed by alignment, consisting of several steps on its own, described as the Procrustes algorithm [24]. Firstly, the centroids of both ${}^{Is}p$ and ${}^{It}p$ are calculated and subtracted from all points in their corresponding point sets so the two point sets are centered in the origin. Secondly, the calculation of the rotation is done with the Kabsch algorithm, which estimates the rotation matrix based on singular value decomposition (SVD). The final step for the alignment is to calculate the translation vector, to obtain the 4×4-transformation matrix ${}^{It}_{Is}T$.

Lastly, error measurement is done by calculating the fiducial registration error (FRE), described as the root mean square (RMS) of the distance between ${}^{It}p_n$ and the transformed ${}^{Is}p$ [24]:

$$FRE = \sqrt{\frac{1}{N}\sum_{n=1}^{N} ||{}^{It}p_n - {}^{It}_{Is}T\,{}^{Is}p||^2} \tag{3}$$

However, the FRE is not an objective measure, as the fiducials that are used for finding the transformation are also used for the evaluation of the registration. Besides, it is more important to know the registration accuracy of the 'targets', which are points that are directly associated with the reason for registration, expressed with the target registration error (TRE). The TRE is defined as the distance between any point in ${}^{It}\varphi$, not used for registration, and their corresponding transformed point from ${}^{Is}\varphi$ with ${}^{It}_{Is}T$. The TRE varies based on the position of the targets relative to the fiducials, where larger distances usually result in higher TRE values [26]. The RMS of the found TREs is calculated to get a single performance measure [24]:

$$TRE_{RMS} = \sqrt{\frac{1}{N}\sum_{m=1}^{N} TRE_m^2} \tag{4}$$

1.2.4 EM-tracked US for surgical navigation

US imaging uses high-frequency sound waves, generated by a transducer, to produce two-dimensional (2D) cross-sectional anatomy images [27]. The transmitted sound waves reflect off boundaries between different tissues, producing echoes that are detected by the transducer's piezoelectric crystals. The speed of sound in tissue (about 1540 m/s) is used to calculate distances, providing real-time, non-invasive imaging.

For surgical navigation, the US probe needs to be tracked with an EM sensor. The most convenient way to achieve this is by designing a clip-on with an EM sensor, securely fitting the US probe. US calibration correlates pixels in US images to the EM sensor. One method for US calibration is proposed by Bo et al. [28], using the tip of an EM-tracked pointer for landmark-based registration. The calibration aims to find the 4×4 transformation matrix describing the rotation and translation from the US-probe reference frame, ${}_{USp}\varphi$, to the US sensor reference frame, ${}_{USs}\varphi$, noted as ${}^{USp}_{USi}T$ (Fig. 5).

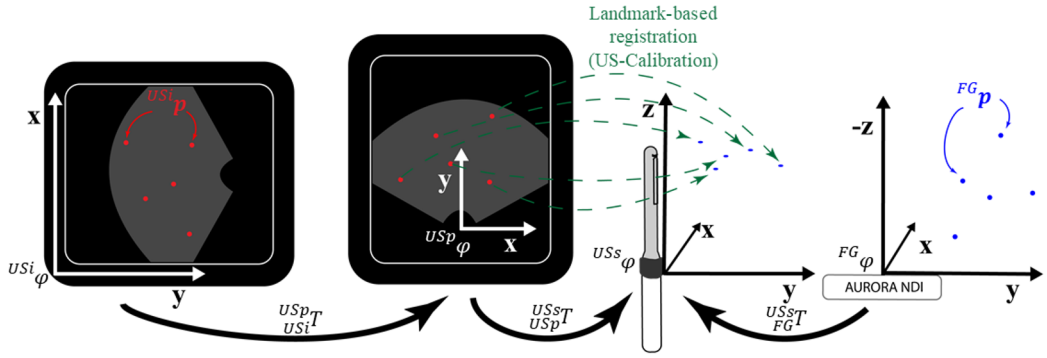

Figure 5. Schematic overview of US calibration transformation matrices.

Four coordinate systems are correlated (Fig. 5). 1) The US image coordinate system ${}_{USi}\varphi$, with its origin in the left upper corner of the US image, 2) the US probe coordinate system ${}_{USp}\varphi$, with its origin in the center of the US probe imaging array, 3) the US sensor coordinate system ${}_{USs}\varphi$, with its origin in the US sensor in the clip-on tool, and 4) the EM coordinate system, ${}_{FG}\varphi$. By imaging the EM-tracked pointer's tip in a basin with a 9.5% ethanol/water solution, with a speed of sound of 1540 m/s mimicking soft tissue, its position is known in two coordinate frames: by its pixel location in ${}_{USi}\varphi$, ${}_{USi}p$, and by the EM data in ${}_{FG}\varphi$, ${}_{FG}p$, correlated by the relationship described in Equation 1.

Following Equation 1, ${}_{USi}p$ is transformed to ${}_{USp}\varphi$ with the transformation matrix ${}^{USp}_{USi}T$, containing rotation and translation based on the origin of the probe on the US screen and a scaling factor based on the current zoom factor of the US device. Additionally, ${}_{FG}p$ is transformed to ${}_{USs}\varphi$, with a transformation matrix ${}^{US}_{FG}T$, acquired by the EM data of the US sensor.

Thereafter, landmark-based registration with ${}_{USp}p$ and ${}_{USs}p$ enables the calculation of the calibration matrix ${}^{USp}_{USi}T$, by using the iterative closest point algorithm described in 1.2.3.

1.2.5 Software and user interface for surgical navigation systems

Surgical navigation systems often incorporate various views to optimize the physician's understanding of the patient's anatomy. Conventional orthogonal MRI/CT slices are desired as physicians are accustomed to these views [29], but 3D models can be of additional value in complex anatomy cases [12–14, 30]. However, these 3D models are visualized on 2D screens, posing difficulties in spatial comprehension and depth perception [11, 31]. Especially accurate estimation of the distance between surgical instruments and target organs is important for the surgeon. Various conventional techniques have been described to overcome the depth perception problems, such as adjusting lighting, shading, and sizing of the visible objects [31]. Augmented reality is a more cutting-edge technology but requires extra equipment, which is often undesirable in a clinical workflow [32]. A higher sense of depth perception is acquired by manually rotating around visible objects. However, this introduces the necessity of a technician controlling the 3D visualization by following the directions of the surgeon, requiring close collaboration and being prone to miscommunication.

A preliminary, recently submitted study in our institution (Van Aalst, 2023) explored the application of game visualization technology in conjunction with EM-tracked GBT catheter insertion, resulting in enhanced comprehension of 3D models on a 2D screen. By

incorporating two 3D model interfaces, each offering a different perspective, and introducing a virtual camera with a ‘third person view’, in line with or perpendicular to the catheter, users were able to insert the GBT catheters more accurately with respect to the target (Fig. 6).

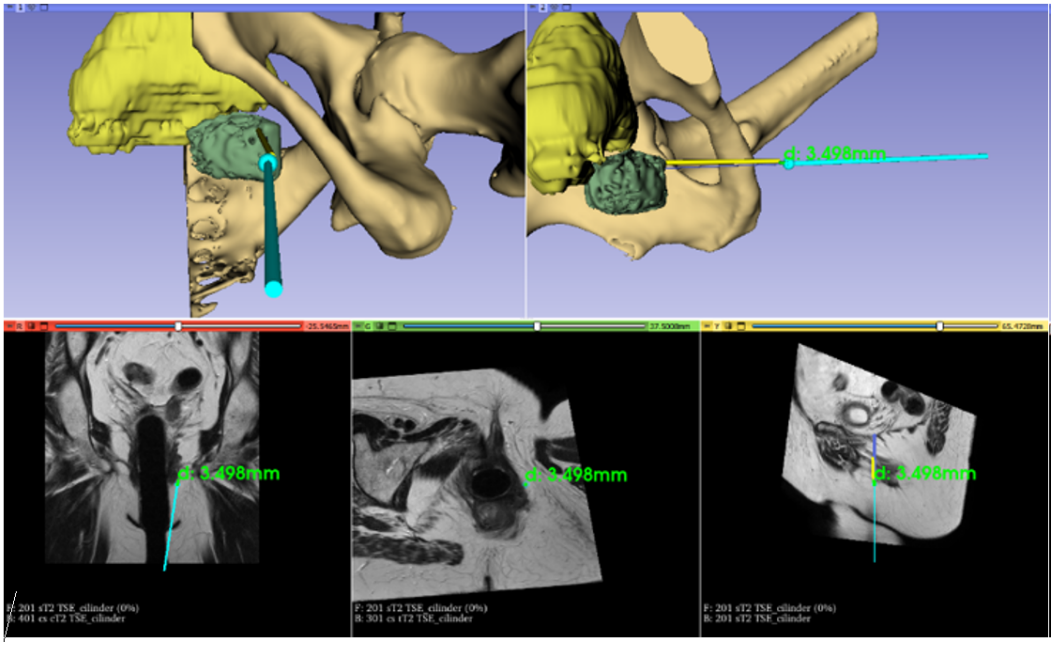

Figure 6. Two automated 3D views with a ’third person’ needle view from behind and from the side. Also, three MRI slice projections are visualized (Van Aalst, 2023).

1.2.6 Clinical research involving non-CE marked medical devices

Surgical navigation systems with in-house developed software and hardware components are considered non-CE-marked medical devices. If such a navigation system is subject to a clinical investigation, involving human participants, official approval by a Medical Ethics Review Committee (MERC) (Dutch: Medisch Etische Toetsings Commissie (METC)) is necessary before starting the study. The Medical Devices Regulation (MDR) [33] is the EU’s regulatory framework for the design and use of medical devices and outlines the requirements for information to be submitted for clinical investigation with a non-CE-marked medical device (MDR Annex XV).

Under the MDR, medical devices are classified into four risk-based classes, ranging from Class I (lowest risk) to Class III (highest risk). This classification system helps regulators, manufacturers, and healthcare professionals to ensure that medical devices meet the necessary safety and performance standards for their intended use. A detailed description of the classification system is provided in MDR Annex VIII. Summarized, the four classes are:

- Class I: Low-risk medical devices that are non-invasive and do not significantly impact the patient’s safety. Examples include bandages, stethoscopes, and non-powered surgical instruments.

- Class IIa: Moderate-risk medical devices that are non-invasive or have limited contact with the patient’s body. Examples include some diagnostic devices, hearing aids, and certain types of surgical instruments.

- Class IIb: Higher-risk medical devices that are invasive and have more significant interactions with the patient's body. Examples include implantable devices, infusion pumps, and orthopedic implants.
- Class III: High-risk medical devices that are invasive and may have life-sustaining or life-supporting functions. Examples include heart valves, pacemakers, and neurostimulators.

For a structured description of all necessary information, the researcher composes a standard Investigational Medical Device Dossier (IMDD), which is submitted to the METC together with the research protocol and other relevant documents.

An important criterion for approval of using the navigation system is close collaboration with the institution's Clinical Physics and Informatics (CPI) and the Decontamination, Sterilization, and Medical Devices Hygiene (DSMH) department. CPI ensures the safe and effective use of the medical device and reviews the medical device for risks of technical or mechanical failure of the software and hardware components. The DSMH ensures proper cleaning, disinfection, and sterilization of medical devices before use on patients and reviews the risks of transmission of infections caused by a medical device. To obtain approval from the DSMH, medical devices must demonstrate full sterilizability. This involves minimizing lumens and fringes in the design and using materials resistant to high autoclave temperatures and Sterrad sterilization [34].

1.3 Rationale

Accurate placement of freehand GBT catheters can be challenging and time-consuming [5, 6, 8, 9]. Using US guidance can be fast and safe, but images sometimes have low contrast, are hard to interpret, and are operator-dependent [35, 36]. The catheters are relatively clearly visible on CBCT, but CBCT is inconvenient to use in the operation room (OR), as it needs a lot of space, and the operating staff needs to leave the OR because of the radiation, disrupting the surgical workflow [37]. Besides, anatomical borders within the pelvis are difficult to identify in CBCT.

With an EM navigation system, it is possible to visualize the catheter in real-time, relative to the patient's anatomy. EM tracking could, therefore, be a valuable addition to the catheter placement workflow [15, 16, 19]. Some phantom studies have successfully used EM tracking to place a BT catheter in a target, with an accuracy of around 2 or 3 mm [22]. Besides, EM tracking for interstitial BT has been investigated for catheter reconstruction after catheter insertion in dose planning [38]. However, in clinical situations, the registration between preoperative and intraoperative imaging is challenging in the pelvic area, mainly due to the deformations of the pelvic organs, because of the difference between preoperative and intraoperative leg positions and the physiological movement of pelvic organs, such as bladder filling. To minimize the effects of these movements, the registration should be based on structures close to or in the tumor.

For external beam radiation therapy (EBRT) registration purposes, three gold markers (GMs) are inserted inside the patient's cervix. These GMs are visible with CT, CBCT, MRI, and US and could, therefore, be used as registration points [39]. To optimize the workflow, US is the desired intraoperative imaging modality used for registration. In this study, we aim to develop and evaluate an EM tracking system (EMTS) for 3D assistance during GBT catheter placement.

2 Materials and methods

An EM navigation system was developed for navigated insertion of EM-tracked freehand GBT catheters. The intended setup with hardware and software components and the proposed clinical workflow are described in this section. For validation of the system and the workflow, the accuracy of different navigation system components was tested, phantom tests were executed, and a clinical case study was conducted.

2.1 Navigation System Description

2.1.1 Set-up

An in-house developed, US-based EM navigation system was designed. The navigation system consists of (Fig. 7):

- An EMTS (Aurora, NDI [17]), with an FG, a sensor interface unit (SIU), a system control unit (SCU) (Fig. 20), a 6DOF FlexTube sensor (Fig 8), and a host computer, all housed in a navigation trolley,
- A BK5000 US system (BK Ultrasound Systems, Analogic Corp., Peabody, MA, USA), with an EM-tracked transrectal US (TRUS) transducer (Fig. 9),
- An in-house designed, EM-tracked stylet for catheter insertion (Fig. 10),
- Dedicated software for preoperative planning, intraoperative visualization, and post-operative analysis.

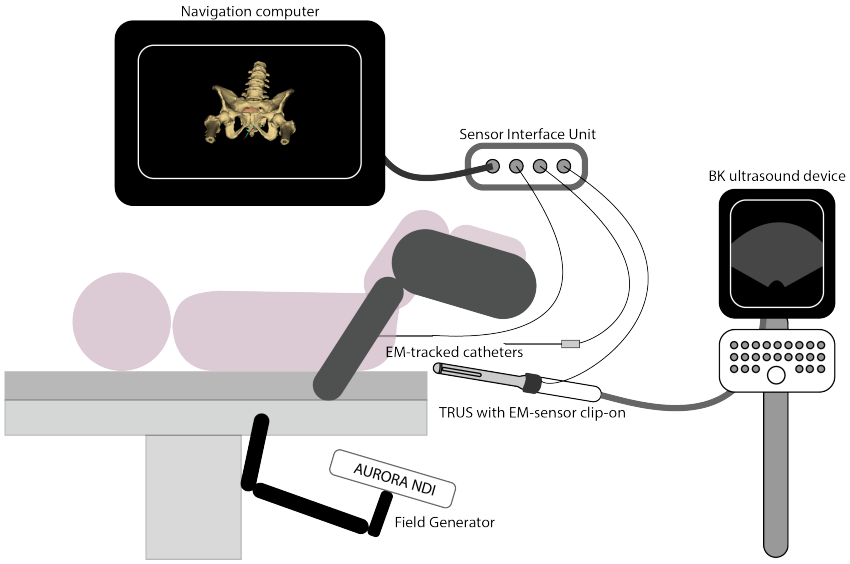

Figure 7. Setup for the EM navigation system with an FG, EM-tracked TRUS, a US device, EM-tracked catheters, a sensor interface unit, and a navigation computer [17].

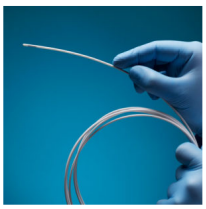

Figure 8. Aurora NDI 6DOF FlexTube [17]

EM Tracking System

The Aurora planar FG (20x20x7.1 cm) has a tracking volume of 50x50x50 cm, in which wired EM sensors detect the varying EM field. The sensors connect to an SIU, which is connected to the SCU, along with the FG. The SCU is linked to the navigation computer, where dedicated software is stored for visualization and analysis.

The reported average position and orientation accuracy of this FG within the measurement volume are approximately 0.70 mm and 0.20 degrees, respectively, for 5DOF sensors and 0.48 mm and 0.30 degrees for 6DOF sensors. However, the accuracy varies, with higher accuracy closer to the FG and reduced accuracy further away. Besides, for each sensor, a specific accuracy corrective factor is reported [16, 17].

EM-Tracked US

A 3D printed clip-on tool of the material Grey V4 with an integrated 6DOF sensor was designed specifically to track the endocavity biplane E14Cl4b US transducer (Fig. 9). All edges of the clip-on tool were blunt to prevent damage to the sterile cover. To relate the US images to the US sensor, US calibration was performed according to the method of Bo et al. [28], described in 1.2.4.

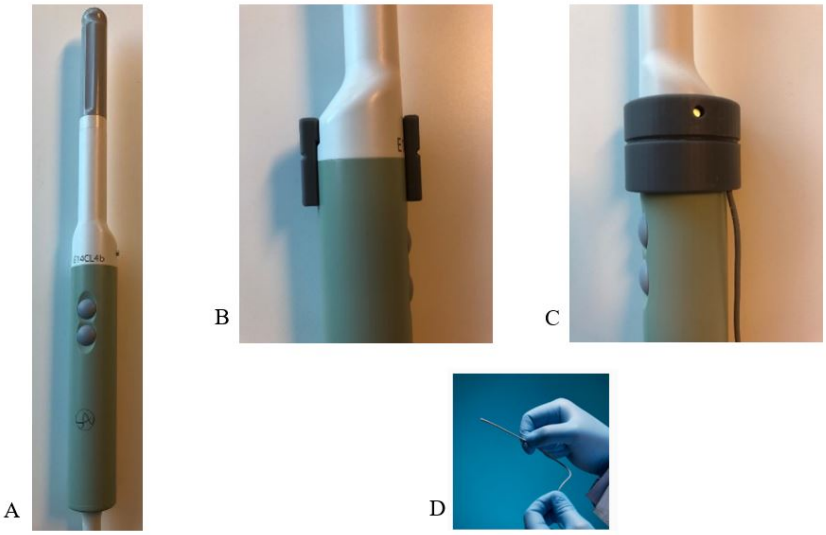

Figure 9. The E13CL4b transducer for the BK5000 US system (A) with a 3D printed clip-on, viewed from the left and from the right side (B, C), and the sensor integrated in the clip-on (D)

EM-Tracked Insertion Stylet

An EM-tracked stylet was designed and produced in-house (Fig. 10, Fig. 11). The stylet consists of a stainless steel 304 tube (1.5 mm outer diameter) with an Aurora NDI 5DOF sensor (0.45 mm diameter, 6.3 mm length) integrated into the tip, and a 3D printed hollow grip made of the sterilizable material BioMed Clear. The sensor's cable was soldered to a silicon-shielded cable with a tool connector containing an SROM device connector (Aurora NDI). All hollow parts were filled with glue (UHU plus schnellfest [40]), and the grip was sealed with a cap and cable gland to facilitate the cleaning process (Fig. 11). All edges were sanded smoothly to reduce contamination risks. The stylet can be sterilized with Sterrad 100NX. The stylet was calibrated with a pivot calibration in Cygna 6D (NDI [17]) while inserted in a catheter, to calibrate the actual tip of the catheter. The RMSE of the calibration was 0.23 mm.

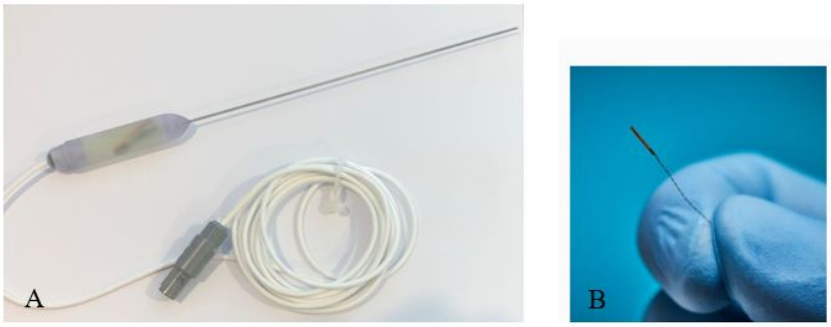

Figure 10. Design for the EM-tracked stylet (A) and the 5DOF sensor integrated into the tip of the stylet (diameter: 0.45 mm, length: 6.3 mm) (B)

The EM-tracked stylet is a reusable surgically invasive device intended for transient use, with connection to an active device, and is therefore classified as class IIa according to rule 6 of MDR annex VIII, being a moderate-risk medical device. Manufacturers of class IIa medical devices must undergo a conformity assessment involving a notified body to demonstrate compliance with essential requirements outlined in the MDR. Additionally, comprehensive technical documentation, clinical evaluation, and a quality management system are required if CE marking is intended.

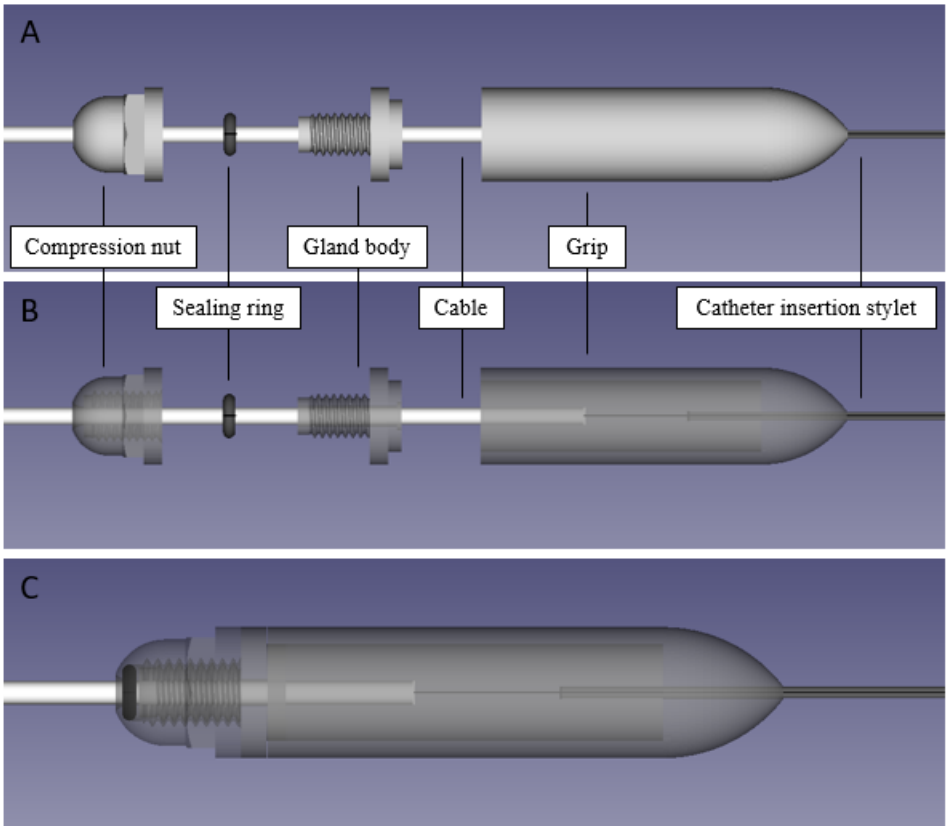

Figure 11. The cable gland and grip design for the EM-tracked insertion stylet. A and B show the individual parts before assembly, with A) the normal view, and B) a transparent view. C) shows the assembled body of the insertion stylet. The compression nut, gland body, and grip were 3D printed. When driving the gland body in the compression nut, the sealing ring is compressed in the compression nut, putting pressure on the cable, fixating it in the compression nut, and making a water-tight connection.

Software
Data of the EMTS and the US imaging were integrated into the open-source software 3D Slicer 5.2.2 [41]. The hardware-to-software connection is established through open-source software PlusServer [42].

Besides the image-guided therapy (IGT) [43] extension within 3D Slicer, two modules were designed to simplify the technical procedure. These modules are designed for scene initialization ('preparation'), and to optimize the user interface and point of view during catheter insertion ('Brachy_set_camera'). These modules are explained in Appendix A.

Preliminary, recently submitted work in our institution showed that the use of two interfaces with automated virtual camera positioning driven by the tracked catheter was intuitive and that the catheters were placed more accurately than with only one, stationary interface.

The software was intended to provide information used to make decisions with therapeutic purposes and could therefore also be classified as a class IIa medical device according to rule 11 of MDR Annex VIII.

Postoperative measurements were also done in 3D Slicer.

2.2 Navigation Workflow

This paragraph outlines all steps necessary for successful EM navigation for GBT catheter insertion, with active tumor tracking. One note has to be made that the workflow has not yet entirely been performed because no eligible patients were scheduled in our institution yet.

2.2.1 Preoperative
Days before the procedure, 3D models of the pelvic structures and organs, including the target lesion, are segmented from the MRI that is acquired one week before the GBT (T2-weighted Turbo Spin Echo) (Fig. 16). The GMs, inserted during an earlier hospital visit for accurate EBRT delivery, are localized in the MRI. The GMs are used intraoperatively for landmark-based registration from US to MRI. The impact of pelvic organ movement on the accuracy might be less significant, as the GMs are placed in close proximity to the target lesion. The use of the Gold Anchor (Gold AnchorTM [44]) markers is preferred over the conventional GMs (VisicoilTM [45]), because the Gold Anchors fold during insertion and therefore anchor in the tissue, decreasing the chance of migration or falling out (Fig. 12). Besides, increased visibility in MRI and US is reported for the Gold Anchor markers [39, 46, 47].

Figure 12. Folded placement of a Gold Anchor [44].

Nevertheless, in case of problems localizing the markers in MRI, supplementary verification is attained by performing a comparative analysis of marker positions in (CB)CT scans, acquired during an earlier hospital visit (Fig. 13). The models are uploaded to 3D Slicer on the navigation computer, in a predesigned startup scene to facilitate the intraoperative navigation procedure.

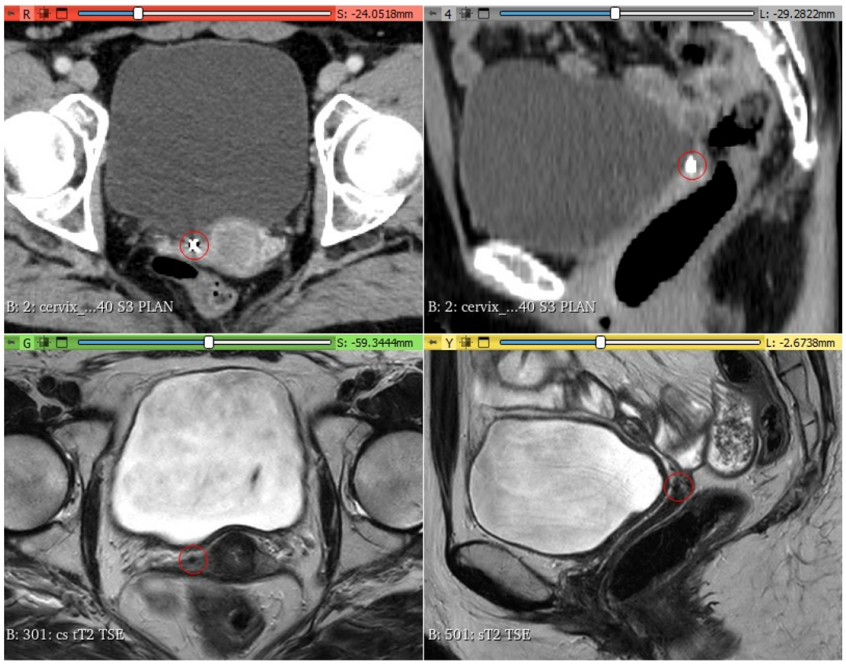

Figure 13. GMs in corresponding slices in CT (upper two views) and MRI (bottom two views). The GMs are indicated with a red circle.

2.2.2 Intraoperative

Preparation

After the patient is anesthetized and positioned in the leg supports, the Aurora Planar FG is mounted below the bed. To compensate for FG movements during the procedure, a 6DOF patient reference sensor is attached to the patient's back, at a location with the least movements due to leg repositioning. All EM sensor's locations are expressed relative to this reference sensor, according to:

$$\begin{aligned} {}^{Ref}_{Cath}T &= {}^{FG}_{Cath}T \times {}^{Ref}_{FG}T \\ {}^{Ref}_{USs}T &= {}^{FG}_{USs}T \times {}^{Ref}_{FG}T \\ {}^{Ref}_{FlexTtube}T &= {}^{FG}_{FlexTtube}T \times {}^{Ref}_{FG}T \end{aligned} \tag{5}$$

Afterwards, the surgical field is covered, and the RTO proceeds with the sterile procedure.

Image Registration

Landmark-based registration is performed using the GMs as landmarks to find a 4x4 transformation matrix that describes the rotation and translation from the reference sensor reference frame, ${}_{Ref}\phi$, to the MRI field reference frame ${}_{MRI}\phi$, noted as ${}^{MRI}_{Ref}T$ (Fig. 14).

Firstly, the GMs are localized by the EM-tracked TRUS in ${}_{Ref}\phi$ (Eq. 5 The GMs are ordered in accordance with the GMs in the MRI, ${}_{MRI}p$. As there are only three GMs, automatic point matching does not give accurate results, so manual point matching is the most robust way.

Secondly, the transformation matrix, ${}^{MRI}_{Ref}T$, is calculated, according to the Procrustes algorithm (section 1.2.3). With that, the objects in ${}_{Ref}\phi$ were transformed to ${}_{MRI}\phi$, enabling an overlay of MRI and US. The transformations applied to the US image and the insertion stylet are:

$$
\begin{aligned}
{}^{MRI}_{USi}T &= {}^{USs}_{USi}T \times {}^{Ref}_{USs}T \times {}^{MRI}_{Ref}T \\
{}^{MRI}_{Cath}T &= {}^{Ref}_{Cath}T \times {}^{MRI}_{Ref}T
\end{aligned}
\tag{6}
$$

The FRE of this initial registration (Eq. 3) is calculated for registration accuracy measurement, noted as FRE_{init}.

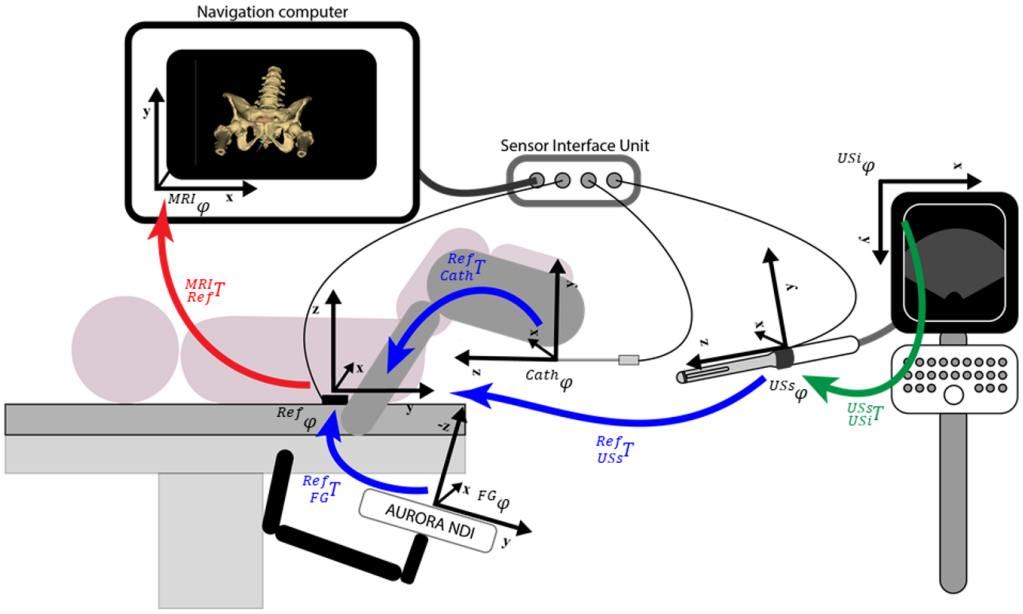

Figure 14. A schematic overview of the transformations that were done in the navigation workflow.

Tumor Tracking

A tumor tracking mechanism is incorporated as the pelvic organs and structures are deformable, causing inaccurate navigation when the RTO adds pressure to the cervix with the US transducer or with a catheter. The first freehand catheter is placed with the EM-tracked insertion stylet by the RTO. After withdrawal of the insertion stylet, the 6DOF FlexTube sensor is inserted into the catheter and fixed with sterile tape. The GMs are visualized again and marked in ${}_{FlexTube}\phi$, by transforming the US image according to:

$$
{}^{FlexTtube}_{USi}T = {}^{USs}_{USi}T \, {}^{FlexTube}_{USs}T
\tag{7}
$$

${}^{FlexTube}_{MRI}T$ is calculated according to Equation 1 and 2, and the Procrustes algorithm described in section 1.2.3 (Fig. 15).

Catheter Insertion

The subsequent freehand catheters are inserted with the EM-tracked insertion stylet, visualized real-time, relative to the FlexTube sensor and thus relative to the moving target area. To optimize the user experience, five interfaces are shown, of which two 3D interfaces, the US image interface, and two 2D MRI slice interfaces (Fig. 16, Fig. 17, Fig. 18). The first 3D interface shows a global view of the 3D models, and the second 3D interface shows a 'catheter view', either in line with or perpendicular to the needle, where the camera moves along with the needle movements. Previous preliminary research in the NKI has shown that having two 3D interfaces gives a clearer view of the 3D structures, on a 2D screen (Van Aalst, 2023). The 2D MRI interfaces convey one axial view, one sagittal view,

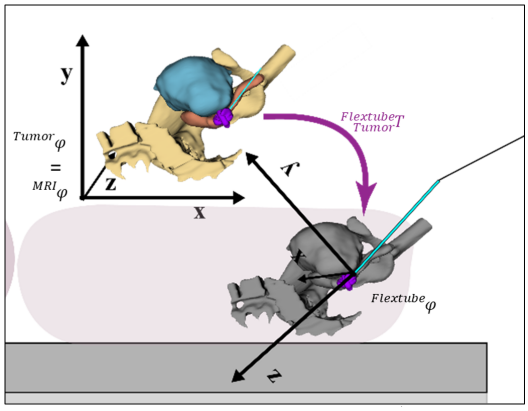

Figure 15. A visualization of the tumor tracking transformation.

and one in-plane needle view. The catheter is displayed with a targeting line, displayed in red in Figure 16, indicating the direction of catheter insertion. Preoperatively planned catheter paths are visualized to serve as insertion guides. Besides, a breach warning module displays the distance from the catheter tip to the target lesion, or from the catheter tip to the preoperatively planned path (Fig. 17). After insertion, the catheter paths are visualized with a margin of 5 mm, to provide insight into dose tumor coverage (Fig. 18).

The US- and EM data are recorded during the procedure for postoperative analysis. The procedure is evaluated with the outcome measures FRE_{init} and $FRE_{\text{TumorTracker}}$. Besides, the TRE (Eq. 4) is calculated by comparing the distances between the catheters and surrounding organs for both the EM-reconstructed catheters and the MRI-reconstructed catheters.

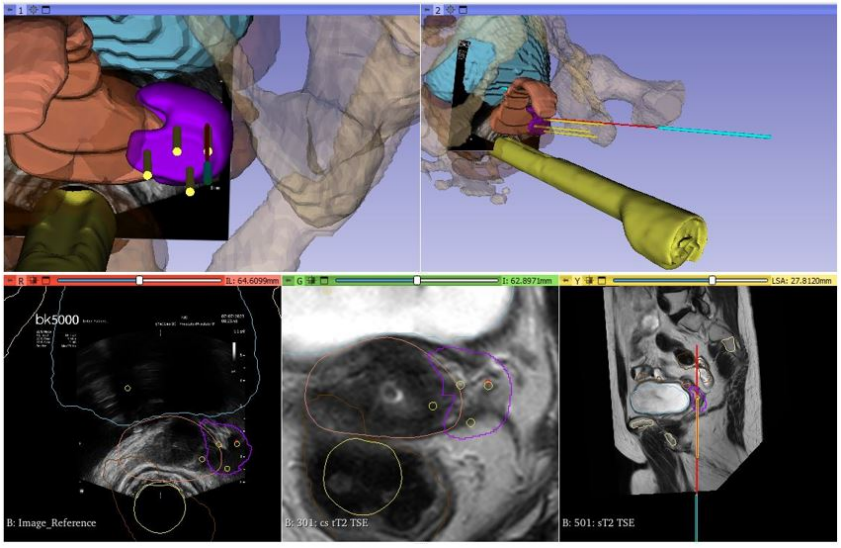

Figure 16. The navigation interface in 3D Slicer with a pelvic 3D model containing a uterus (pink), tumor (purple), bladder (blue), bones (beige), the TRUS transducer, the preoperatively planned catheter paths (yellow), and the real-time visualized catheter (blue) with a targeting line (red). The left upper view displays the third-person catheter view, and the right upper view displays the 3D global view. In the red interface, the US is displayed with an overlay of the 3D model. The green interface displays the axial MRI view and the yellow interface the in-plane view, both with the segmented organs, indicating where the catheter will be placed by the red circle/line.

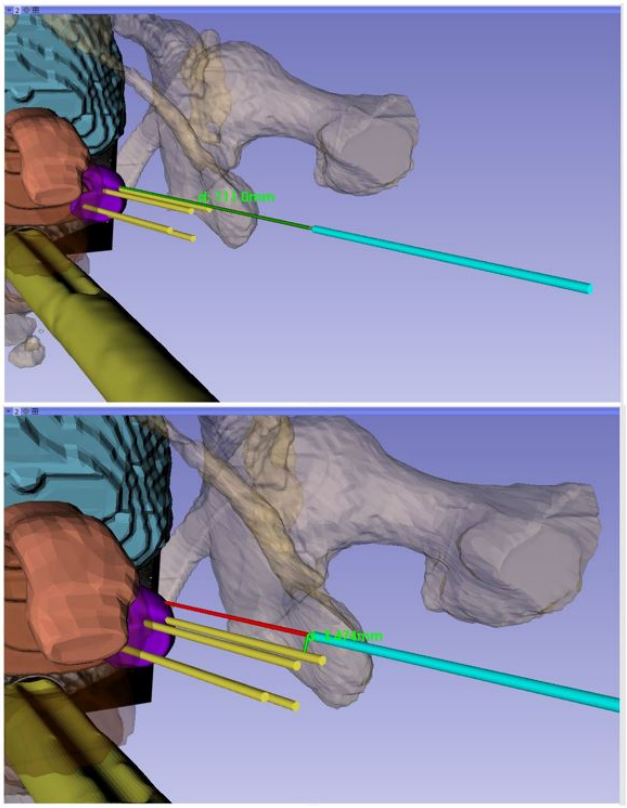

Figure 17. A visualization of the breach warning module, the upper view shows the distance from the catheter to the tumor, and the lower view shows the distance from the catheter to the closest preoperatively planned path.

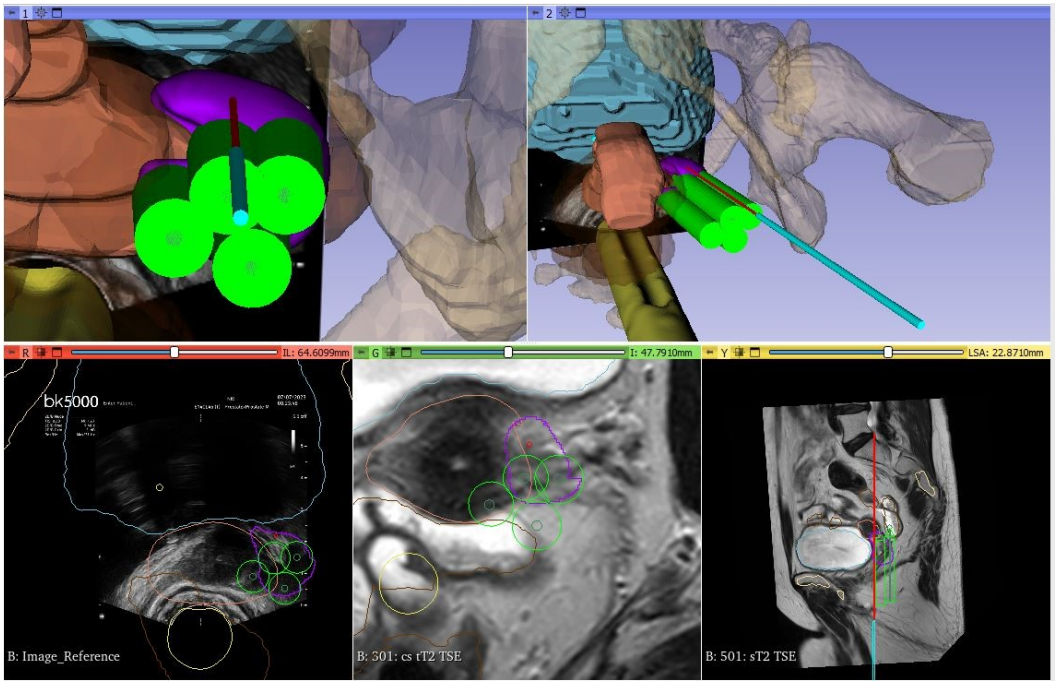

Figure 18. The navigation interface after catheter insertion. Four inserted catheters are displayed in dark green, with a margin of 5 mm in light green.

2.3 Accuracy Tests

2.3.1 EM System Accuracy

The EM tracking system underwent testing in a clinical environment, using a method based on a standardized test proposed by Hummel et al. [48] (Fig. 19). The test setup involved a clinically used OR bed with a metal reduced bed insert, two leg supports, and the Aurora NDI planar FG. A plate with 8 6DOF sensors, fitting a box with a grid of 10x7 positions with a spacing of 5 cm, resulted in a measurement grid of 35x45x30 cm. The NDI track software was used for measurements.

Per sensor location, 150 measurements were averaged to get one mean position and orientation. The obtained grid was registered to a virtual grid in Matlab 2023a using an iterative closest point algorithm. The positional errors were calculated based on the distance between the virtual grid and the sensors, being a measure of the accuracy. The jitter was found by calculating the RMS of the Euclidian distances between the measured locations and the mean location, over all the measurements, being a measure of precision. To obtain clinically relevant measurements, measurements at more than 330 mm distance in the z-direction from the field generator were excluded, resulting in 5 vertical levels.

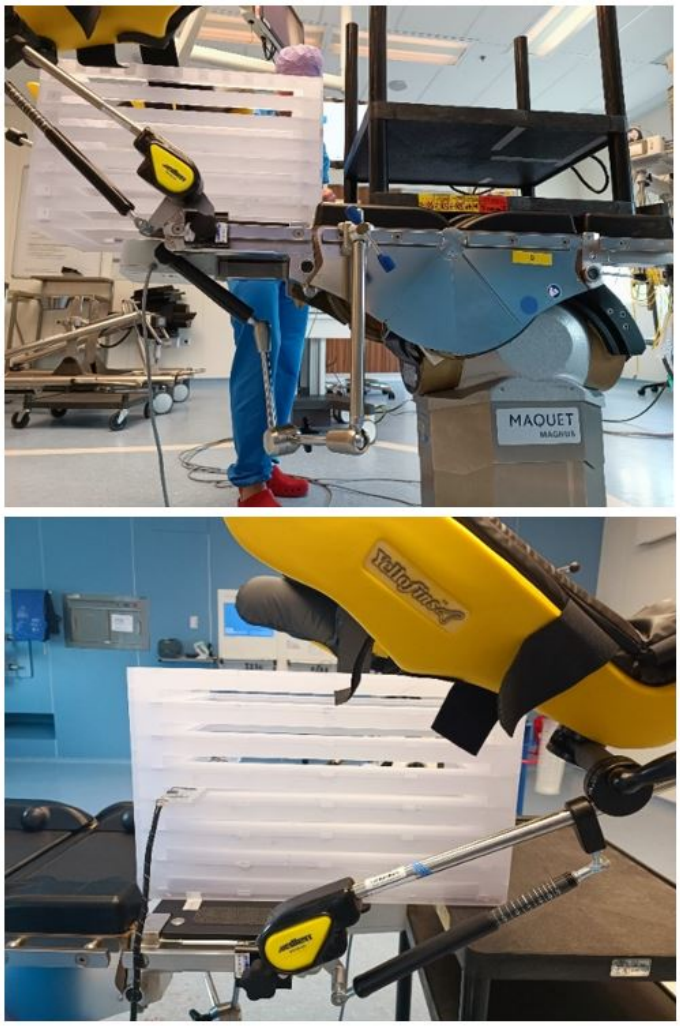

Figure 19. The experimental setup of the Hummel board test [48].

2.3.2 *US Accuracy*

Both the sagittal and the transverse imaging plane of the TRUS were calibrated according to the method of Bo et al. [28], section 1.2.4. To quantify the accuracy of the EM-tracked TRUS, the FRE was calculated (Eq. 3), and the TRE by means of the leave-one-out-method [24]. With this method, the registration is performed again but with one point left out. This point is used for measuring the TRE, which is the Euclidian distance between the transformed US point and the EM point. This is done for all points. Finally, the RMS of the found TREs was calculated to get a single performance measure (Eq. 4).

2.3.3 *Stylet Accuracy*

The accuracy of the EM-tracked stylet was measured by pointing at a known reference point on the Aurora 6DOF reference sensor tool [17] (Fig. 20). A total of 76 points were recorded in different positions in the EM field. The mean and standard deviation of the 76 errors were calculated.

Besides, the angle of the sensor in the tube was measured by spinning around the needle axis, placing fiducials at the tip of the needle p_{tip} and at the end of the needle p_{end}. The angles between all possible combinations of p_{end} and p_{tip} were calculated. The half of the largest angle was assumed as the angle of the sensor in the tip (Fig. 21).

Figure 20. The Aurora NDI 6DOF reference tool (diameter: 25 mm, thickness: 5 mm) [17].

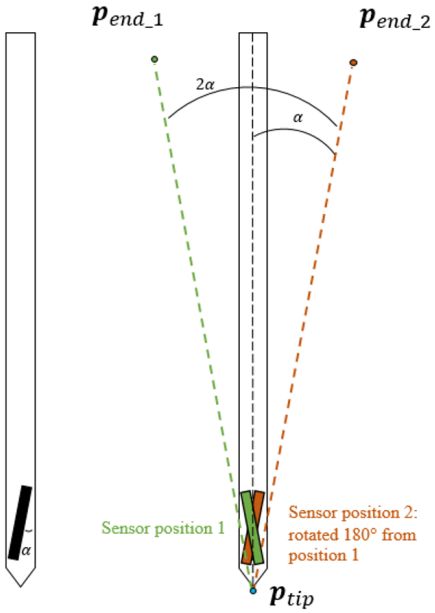

Figure 21. Schematic overview of the measurements of the sensor angle in the insertion stylet.

2.4 Phantom Tests

Phantom tests were conducted to test the initial accuracy and system usability with a prostate phantom containing a rectal wall, seminal vesicles, perineal membrane, a urethra, three lesions, and three GMs (Fig. 22). All structures are visible with (CB)CT, MRI, and US. CBCT served as preoperative imaging, as it was quick and easily accessible. The structures were segmented using 3D Slicer software.

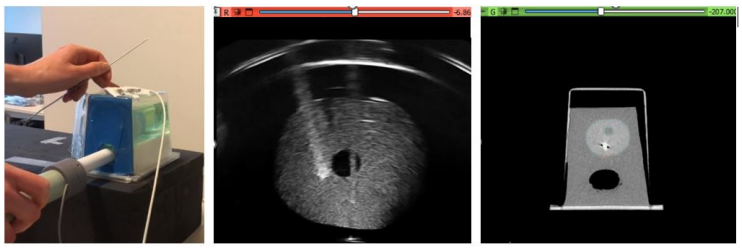

Figure 22. The prostate phantom with the TRUS transducer inserted. The middle view displays a US image and the right view displays a CBCT slice of the phantom, both with a GM.

During the tests, the users located the GMs with the EM-tracked TRUS. Landmark-based registration with the GMs was employed to register the EM field with the CBCT, resulting in the initial FRE, FRE_{init} (Eq. 3). The user placed one catheter and inserted a FlexTube sensor in the catheter, serving as a tumor tracker. Landmark-based registration was performed again with the locations of the GMs relative to the FlexTube sensor, resulting in the tumor tracker FRE, $FRE_{TumorTracker}$. Subsequently, the user placed six catheters. A recorded US sweep was made of the entire prostate. To evaluate the overlay accuracy, the distances between the EM-reconstructed catheters ($Cath_{EM}$) and the US-reconstructed catheters ($Cath_{US}$) were calculated (Fig. 23). The RMS of the shortest distances from fiducials placed along $Cath_{US}$ to $Cath_{EM}$ was calculated as TRE. Additionally, the RMS of the US-tip to EM-tip distance was calculated to quantify the z-direction accuracy of the catheter ($Error_{tip}$).

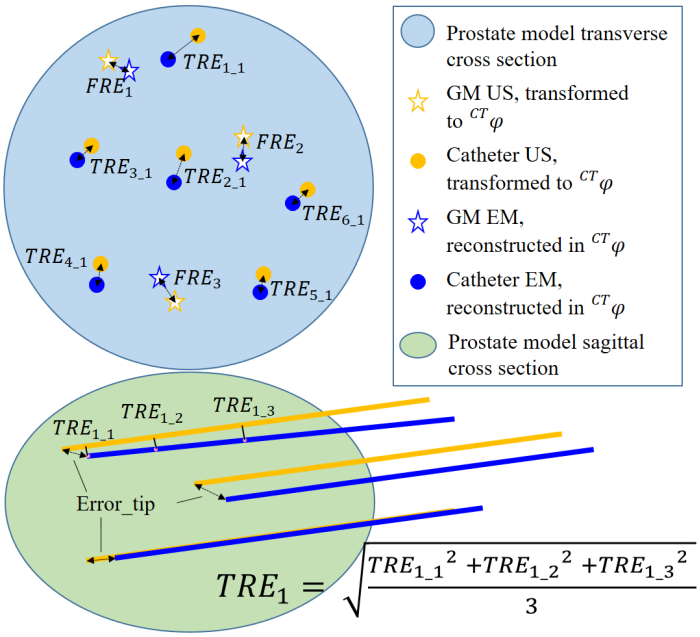

Figure 23. Schematic presentation of the phantom test outcome measures, which are FRE_{init} and $FRE_{TumorTracker}$, TRE, and $Error_{tip}$.

2.5 Case study: The feasibility of EM tracking for GBT catheter insertion

Two patients scheduled for intrauterine BT were included in our case study. The patients underwent regular intrauterine BT, thus a procedure without the placement of freehand catheters. Consequently, only the first part of our proposed workflow could be executed. However, due to the absence of eligible patients with freehand catheters after the METC approval, we proceeded with the regular procedures to gain clinical experience.

3 Results

3.1 Accuracy tests

3.1.1 EM system accuracy

The position error was visualized as a vector at their position in the grid, and the errors were plotted against the distances to the FG (Fig. 24). The mean error was 0.64 mm. The error was higher at larger distances from the FG. Besides, higher errors were seen at the left superior dorsal corner (patient perspective). The mean jitter was 0.02 mm.

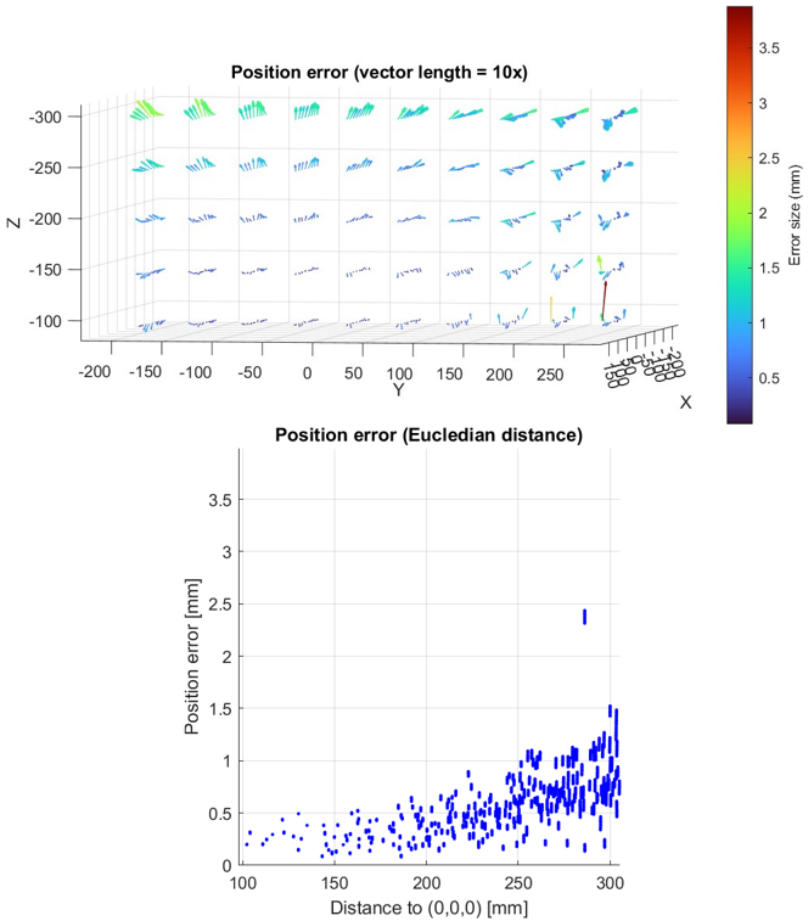

Figure 24. Position error in the EM field in a clinical setup. The upper graph displays the errors at the measurements' positions in the grid. The grid is rotated such that the directions correspond with the directions in the upper image in Figure 19. The lower graph shows the relation between the distance to the FG.

3.1.2 US calibration accuracy

For the transverse US calibration, the FRE was $1.47 \pm 0.65\,\mathrm{mm}$ and the RMS TRE was $1.59 \pm 0.70\,\mathrm{mm}$. For the sagittal US calibration, the FRE was $0.65 \pm 0.32\,\mathrm{mm}$ and the RMS TRE was $0.72 \pm 0.37\,\mathrm{mm}$.

3.1.3 EM-tracked stylet accuracy

The calibration RMS of the EM-tracked stylet was $0.23\,\mathrm{mm}$. The mean position error of the EM-tracked stylet was $0.54 \pm 0.14\,\mathrm{mm}$ ($\mathrm{error}_x = 0.14 \pm 0.07\,\mathrm{mm}, \mathrm{error}_y = 0.51 \pm 0.19\,\mathrm{mm}, \mathrm{error}_z = 0.10 \pm 0.11\,\mathrm{mm}$). The angle of the sensor in the tube was $0.9°$.

3.2 Phantom tests

The phantom tests were executed four times, with three different EM navigation specialists. With six catheters per phantom test, a total of 24 catheters were inserted. The resulting model-US overlay and 3D model view are visualized in Figure 25. $\mathrm{FRE}_{\mathrm{init}}$ and $\mathrm{FRE}_{\mathrm{TumorTracker}}$ for each experiment are displayed in Table 1, the RMS of the $\mathrm{Errors}_{\mathrm{tip}}$, and the mean TRE are displayed in Table 2. The mean FRE for all experiments was $0.83 \pm 0.23\,\mathrm{mm}$ for the initial registration and $0.74 \pm 0.24\,\mathrm{mm}$ for the tumor tracker registration, relative to the sensor in the catheter. The mean overall US-catheter to EM-catheter distance was $1.69 \pm 0.60\,\mathrm{mm}$. The mean US-tip to EM-tip distance was $3.04 \pm 0.72\,\mathrm{mm}$.

Table 1. $\mathrm{FRE}_{\mathrm{init}}$ and $\mathrm{FRE}_{\mathrm{TumorTracker}}$ of the four phantom experiments and the overall mean and standard deviation (STD) (in mm).

Experiment	1	2	3	4	Mean ± STD
$\mathrm{FRE}_{\mathrm{init}}$	0.49	1.09	0.77	0.96	0.83 ± 0.23
$\mathrm{FRE}_{\mathrm{TumorTracker}}$	0.42	1.05	0.85	0.62	0.74 ± 0.24

Table 2. The mean RMS $\mathrm{error}_{\mathrm{tip}}$ and TRE of the four phantom experiments separately and overall (in mm).

Experiment		1	2	3	4	Overall
$\mathrm{Error}_{\mathrm{tip}}$	Mean	3.17	4.25	3.02	4.75	3.04
	STD	± 1.34	± 1.56	± 1.58	± 2.11	± 0.72
TRE	Mean	1.49	2.67	1.55	1.04	1.69
	STD	± 0.77	± 1.07	± 0.67	± 0.41	± 0.60

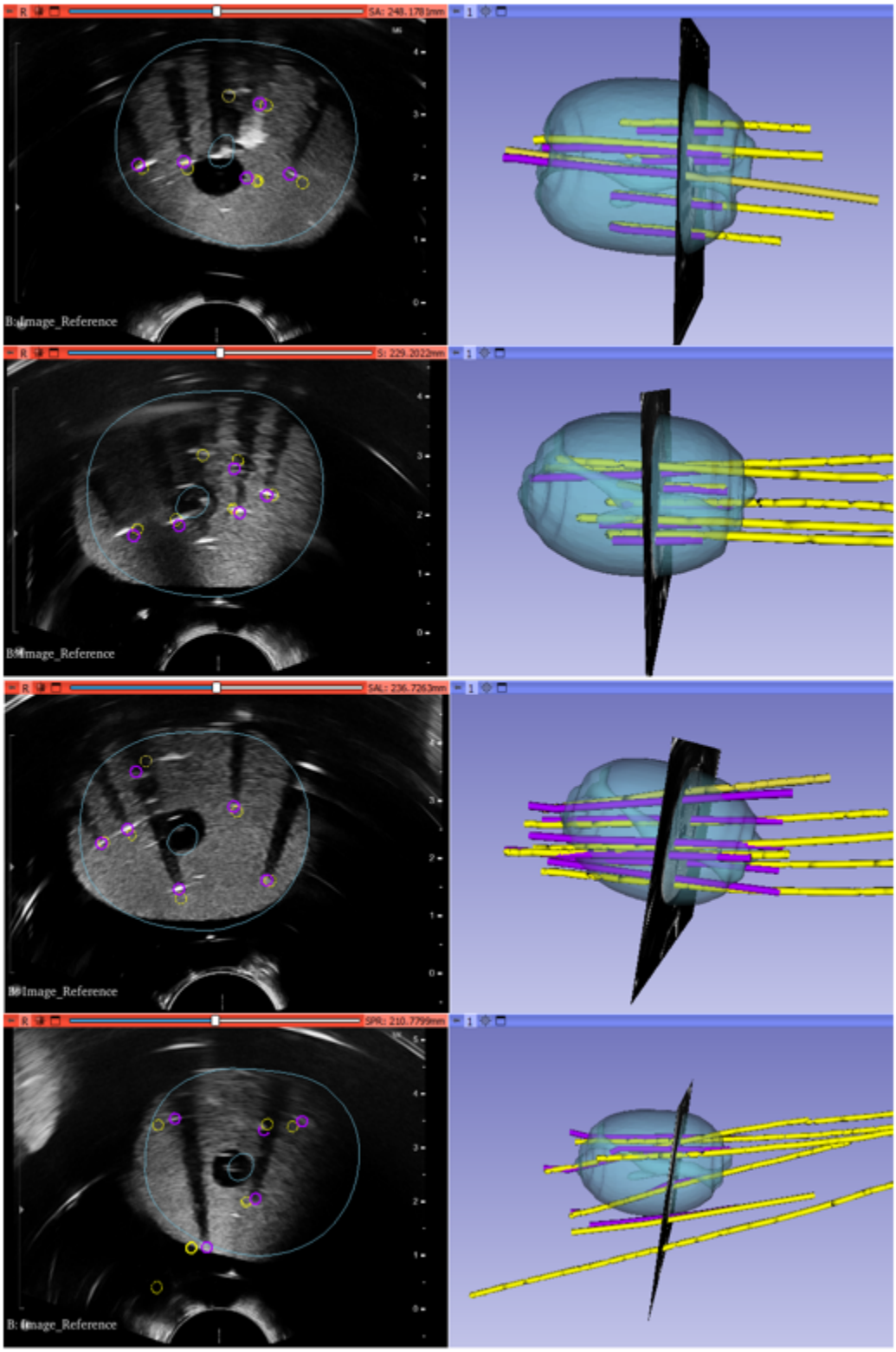

Figure 25. Results of the phantom tests with the US image on the left and the 3D view on the right. The yellow paths are the EM-reconstructed paths and the purple paths are the US-reconstructed paths.

3.3 Case study: The feasibility of EM tracking for GBT catheter insertion

A total of three procedures for two patients were included. Procedure 1 involved the placement of catheters through the applicator. Procedures 2 and 3 only involved insertion of the applicator, without catheters.

The first part of the proposed workflow, described in section 2.2 was followed, including preoperative preparation and image registration. In addition to the MRI 3D model, a second 3D-pelvic organ model was created based on a preoperative CT scan. The bladder filling in this CT scan matched the intraoperative situation better. Therefore, both the GMs in MRI and CT were used to compute the registration.

The GMs were clearly visible in the US images, brightly hyperechoic with a reverberation artifact, as can be seen in the left US image in Figure 26 and in the left US image in Figure 27. This enabled registration with a mean FRE_{init} of 2.4 mm for both the CT-US and MRI-US registration. The FRE_{init} for each procedure is displayed in Table 3.

Upon visual inspection of the overlay, it's clear that the overlay error was bigger than the given FRE (Fig. 26, Fig. 27, Fig. 28). In procedure 1, the CT-US overlay was better than the MRI-US overlay, in procedure 2, the MRI-US overlay was better, and in procedure 3 they were comparable. Quantifying the TRE was challenging due to the absence of clear anatomical landmarks and the rounded nature of the uterus. Consequently, the TRE was not calculated in the study.

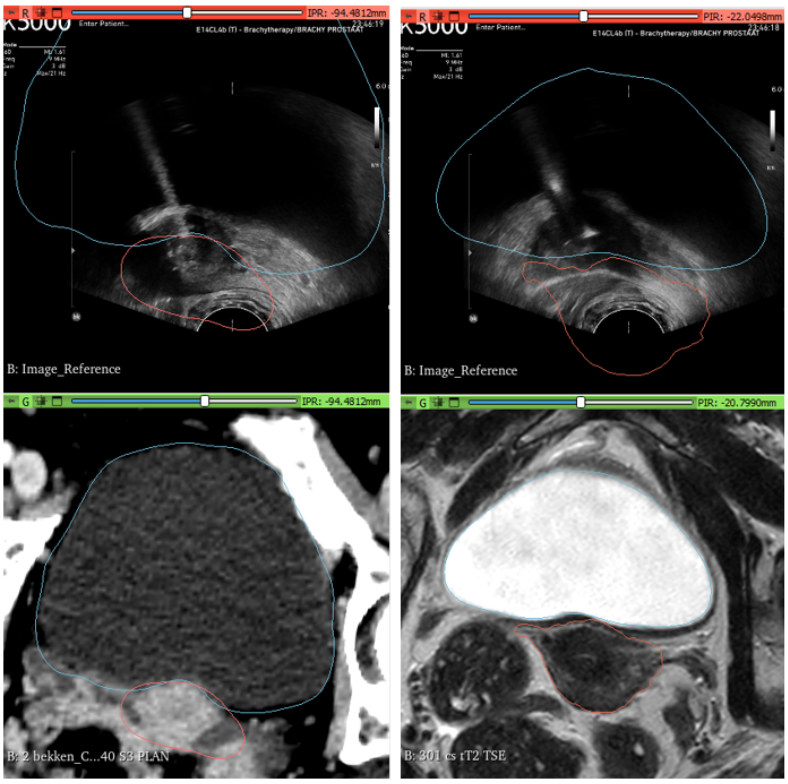

Figure 26. The overlay of the CT model (left) and the MRI model (right) onto a US image after registration, and the corresponding CT and MRI slices with segmented structures, for procedure 1.

Table 3. FRE_{init} values for the MRI-US and CT-US registration in three procedures (in mm).

PROCEDURE	1		2		3		MEAN	
	MRI	CT	MRI	CT	MRI	CT	MRI	CT
FRE_{init}	1.9	2.1	3.1	4.0	2.2	1.2	2.4	2.4

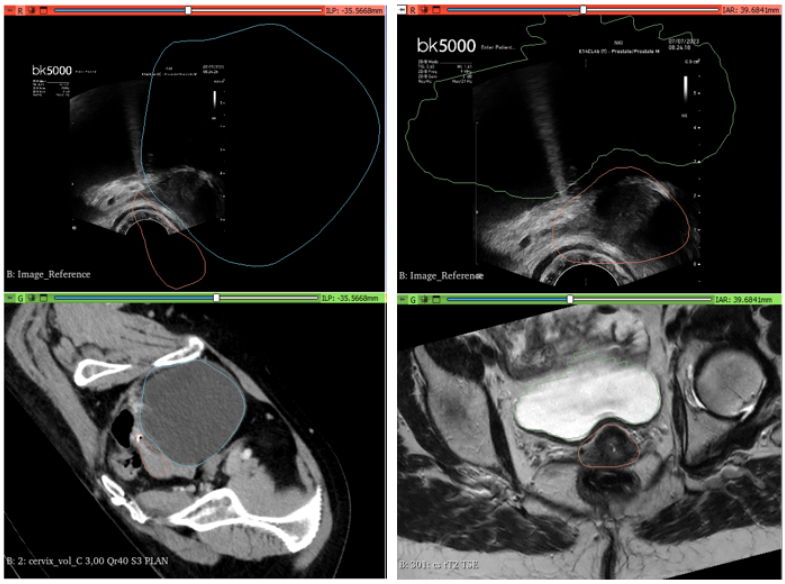

Figure 27. The overlay of the CT model (left) and the MRI model (right) onto a US image, and the corresponding CT and MRI slices with segmented structures, for procedure 2.

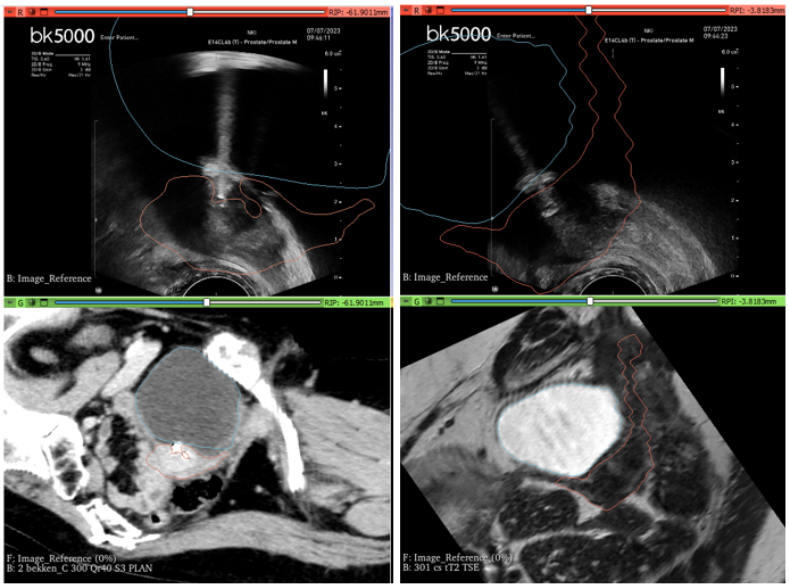

Figure 28. The overlay of the CT model (left) and the MRI model (right) onto a US image, and the corresponding CT and MRI slices with segmented structures, for procedure 3.

The tumor tracking principle was only tested in procedure 1, as procedures 2 and 3 did not involve catheters. Instead of initially placing a freehand catheter, as proposed in our workflow, the catheters were placed through the applicator. A FlexTube sensor was placed in

the first catheter, after which the RTO attempted to localize the GMs again with the TRUS, for tumor tracking. However, the GMs were not visible after the insertion of the applicator, due to emerging artifacts, except for one GM. Therefore, calculating ${}^{\text{Flextube}}_{\text{MRI}}T$ for tumor tracking was not feasible. The one GM that was visible was used to calculate an additional translation between the situation before applicator insertion and the situation after applicator insertion, which was a shift of 29.4 mm. The adjustment improved the overlay (Fig. 29).

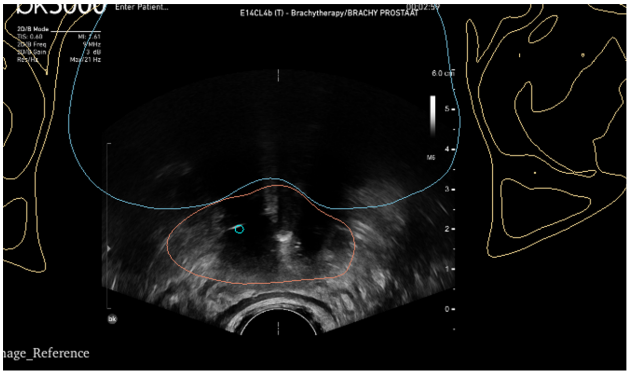

Figure 29. Overlay after insertion of the FlexTube sensor (blue circle) and the extra translation due to insertion of the applicator, based on one GM.

Finally, the FlexTube sensor was inserted inside every catheter to reconstruct the catheters based on EM data (Cath_{EM}) (Fig. 30). The geometry of Cath_{EM} and the MRI-reconstructed catheters, Cath_{MRI} (Fig. 31), matched visually. Besides, landmark-based registration was performed with the tips of Cath_{EM} and Cath_{MRI} as fiducials, resulting in an FRE of 3.5 mm. The CT model was transformed to the postoperative MRI model with the catheter registration transformation matrix (Fig. 32). The distance between the uterus top in the MRI model and the uterus top in the CT model was 1.4 mm. Other distances were not calculated, as the CT showed an over-segmentation of the uterus (ie. more tissue is classified uterus than supposed to), making accurate calculations impossible.

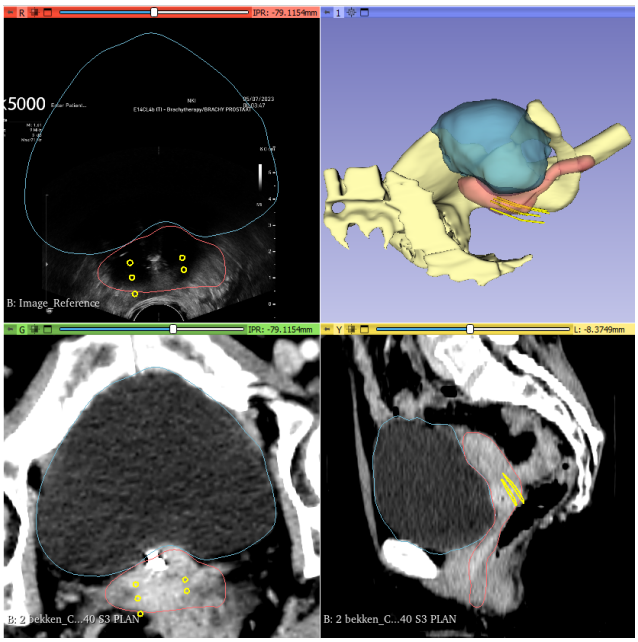

Figure 30. The results of the EM-reconstructed catheters (yellow) projected in the preoperative CT and visualized with respect to the preoperative CT model.

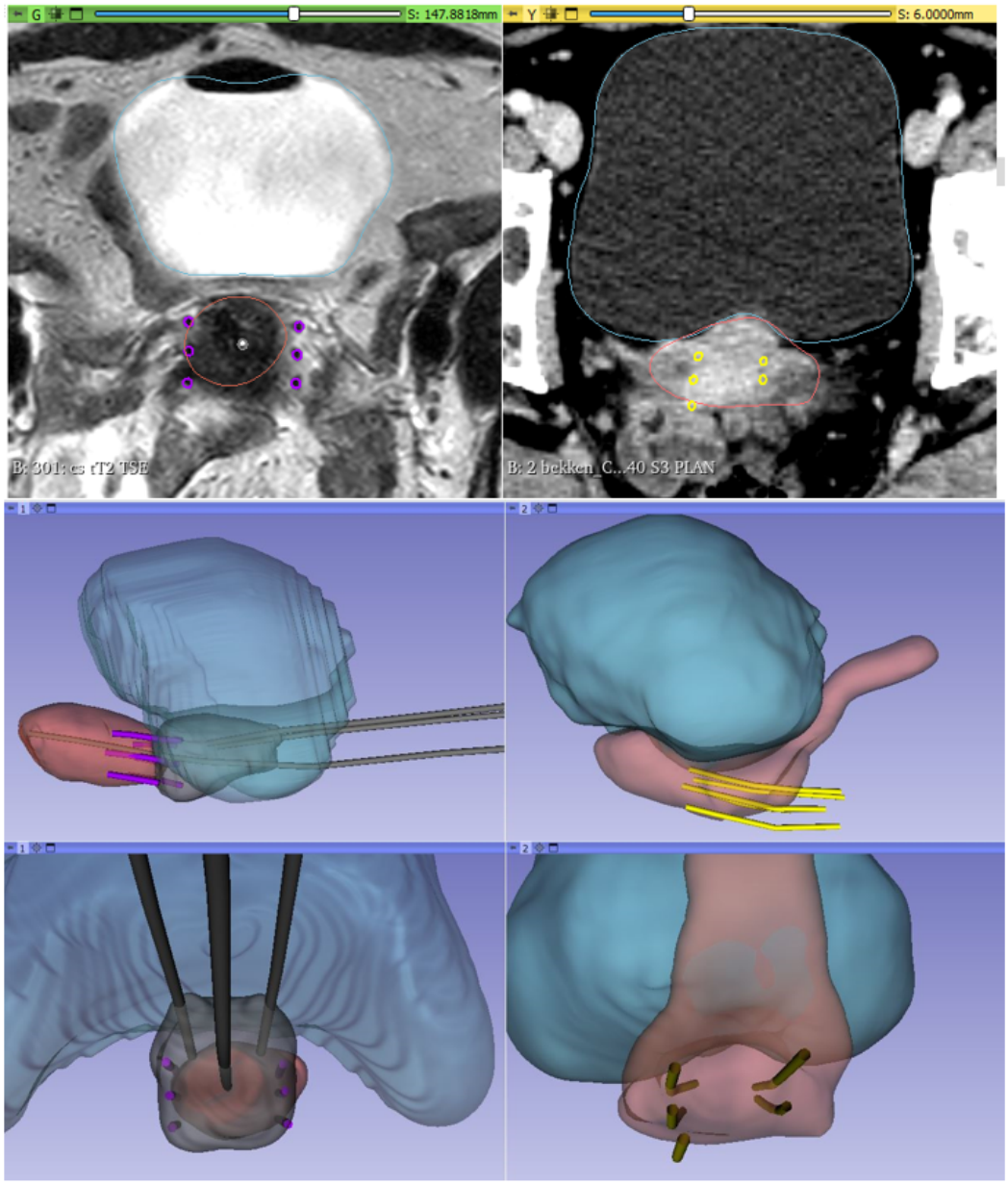

Figure 31. The left images show the postoperative MRI images and models, with the six catheters reconstructed. The right images show the preoperative CT model, with five catheters reconstructed based on the EM data.

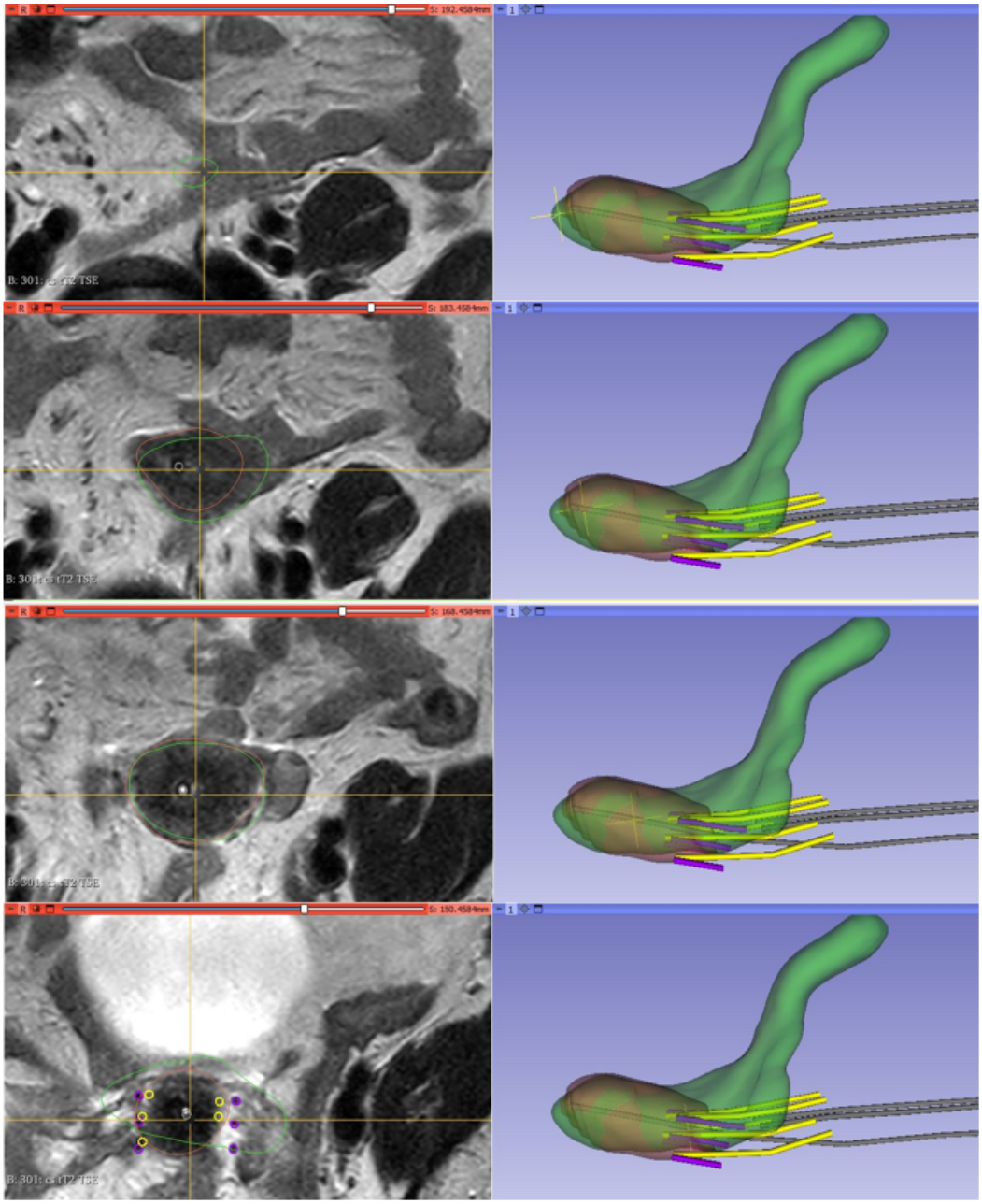

Figure 32. Visualizations of the transformed CT-uterus model, based on the tips of $Cath_{EM}$ and $Cath_{MRI}$. The left images show the 2D slices with the segmented MRI uterus (pink) and the transformed CT uterus (green). The crosshair in the 2D slices and in the 3D model are correlated, indicating the position of the slice in the 3D model.

4 Discussion

This study was conducted to assess the feasibility of EM navigation for GBT freehand catheter insertion. A clinical navigation workflow was designed, incorporating an Aurora EM tracking system, EM-tracked TRUS, and an in-house developed catheter insertion stylet. EM navigation accuracy was evaluated, phantom tests were performed, and the first clinical results were acquired. These results show that EM navigation is feasible in a clinical GBT workflow.

The EM navigation workflow provides several benefits when compared to the current practice. The insertion of freehand catheters is currently done without any real-time visualization, requiring post-insertion verification using CBCT, which disrupts the workflow and increases surgery time. The navigation system provides a better understanding of the patient's anatomy due to the different 3D model views and the 2D MRI slices that are implemented in the navigation interface (Van Aalst, 2023). Furthermore, the insertion stylet can be visualized real-time, and the RTO can align the insertion stylet with preoperatively planned catheter paths. A targeting line projects the catheter's insertion direction, and a "breach warning" module displays the distance from the EM-tracked catheter to the preoperatively planned target. Lastly, the system allows for the reconstruction of the inserted freehand catheters in the MRI model, with a margin of 5 mm, allowing for inspection of tumor dose coverage without the need for CBCT.

EM tracking Accuracy Tests
The Hummel board test demonstrated that the clinical setup hardly introduced field distortions, with an average position error of 0.64 mm, compared to 0.53 mm in a non-distorted environment. Higher errors, up to 2 mm, were observed at greater distances from the FG, as expected [17, 49]. The higher errors at the left superior dorsal corner could potentially be attributed to the metal parts on the bed. However, the error was below 0.5 mm within the clinically relevant area (y -100 to 100 mm and z -100 to -200 mm in Figure 24), providing evidence that the proposed clinical setup will not cause significant distortions in the EM field. However, it must be noted that the sensors used for the Hummel board test were very accurate, with a corrective factor of 0.8, possibly giving optimistic results compared to the clinically used sensors. Nevertheless, the average position error will still be low (around 0.8 mm) when using less accurate sensors. The mean jitter found from the Hummel board test was 0.2 mm, indicating that the sensor's measurements were very precise. Precise results are important for real-time tracking as the sensor's position is constantly measured, thus averaging is not possible.

The US calibration accuracy was comparable to previously conducted studies [28] (FRE axial, sagittal: $1.47 \pm 0.65\,\mathrm{mm}$, $0.65 \pm 0.32\,\mathrm{mm}$, RMS TRE axial, sagittal: $1.59 \pm 0.70\,\mathrm{mm}$, $0.72 \pm 0.37\,\mathrm{mm}$). The EM-tracked stylet had an average position error of 0.57 mm, outperforming previous studies [49]. The angle of the EM sensor in the tube (0.9°) is not expected to introduce any inaccuracies in navigation. The sensor is positioned approximately 13 mm to the tip of the catheter, so an angle of 0.9° results in a positional error of 0.2 mm in the tip. The error in the targeting line of the catheter, at approximately 200 mm from the sensor (i.e. target in tissue when the needle is positioned at the skin), is approximately 3 mm as a result of this sensor angle.

By considering the average Hummel board position error, US calibration error, and EM-tracked stylet position error, a comprehensive estimation of the worst-case scenario error is obtained, yielding an error value of 2.80 mm. This is comparable to EM workflow accuracy results in previously conducted studies [18], and is not expected to introduce any clinical

problems, while the real error will even be lower. This is also shown by looking at the phantom test results, yielding a TRE value of 1.69 mm and an $Error_{tip}$ of 3.04. As the phantom tests were conducted in deformable tissue, which induces an additional error, it can be concluded that 2.8 mm is an overestimation of the total EM tracking error.

Phantom Tests
Phantom tests indicated that the workflow is feasible and accurate ($FRE_{TumorTracker}$: 0.74 ± 0.24 mm, TRE: 1.69 ± 0.60 mm), which is in the range of previously conducted phantom studies, reporting targeting errors ranging from 0.7 mm [21, 50, 51] to 3.4 mm [49, 52]. One important limitation of the accuracy measurements of the phantom study was that the rigid EM-tracked insertion stylet could manipulate the deformable phantom material, leading to potential inaccuracies in reconstruction location. The $Error_{tip}$ was higher (3.04 ± 0.72 mm), where the data often suggested that the EM-reconstructed catheter was inserted further into the tissue than the US reconstructed catheters. This difference could be attributed to the aforementioned limitation, where pressure on the EM-tracked stylet might cause manipulation in the catheter's z-direction, or to the visibility of the catheter's tip in the US images, which could be inaccurate up to 3 mm [53], requiring further assessment.

It is important to realize that the reported measures indicate the accuracy of the EM navigation, and not the accuracy of the catheter placement by the user, following a preoperatively defined line. This study did not measure the accuracy of catheter placement by the user, and the accuracy and time difference between EM-navigated placement and conventional placement. This was decided because the phantom was insufficiently representable for the clinical situation in terms of complexity and echogenicity, probably giving skewed results. Previous phantom studies in our institution, using phantoms that were more suitable for this purpose, demonstrated that catheter placement is more accurate with the use of an EM navigation system than without (Buter, 2022).

Case Study
The aim of the case study was to gain clinical and technical experience for both the technical physicians executing the EM navigation and the RTOs performing the catheter insertion, to test if the tumor tracking principle was feasible after insertion of the applicator, and to get preliminary results of the navigation system. Due to the absence of eligible patients scheduled with freehand catheters in our institution, the case study was conducted with patients undergoing standard GBT catheter insertion procedures without freehand catheters. As a result, only the first part of the proposed navigation workflow could be tested, while an important component for accurate navigation, tumor tracking, was omitted. Nevertheless, we were able to register based on the GMs with relatively high accuracy for soft tissue registration, with a mean FRE_{init} of 2.4 mm for both the MRI-US registration and the CT-US registration. Besides, we were able to reconstruct the catheters based on EM data, with a geometrical accuracy of 3.4 mm.

The correctness of the MRI-US and CT-US overlays varied, with some cases showing better alignment using MRI and others using CT. Several components could influence this variation. Firstly, the overlay was mainly assessed at a cross-section of the uterus body, while the GMs were positioned lower in the cervix. Varying bladder filling at the time of the scans and during the procedure will cause a shift and a rotation of the uterus [3], making the uterus overlay inaccurate, while the cervix and target overlay could be accurate. Furthermore, the visibility of the GMs in the MRI was limited, making the localization and therefore the registration uncertain. Future studies should explore alternative markers or include other MRI sequences to improve the visibility of GMs in MRI for better registration accuracy. The GMs should be better visible on tT2-TSE and T1 3D GRE. These sequences can be

acquired in less than 8 and 4 minutes, respectively, which is acceptable as a prolongation of acquisition time for the patient. Besides, the GMs were inserted in close proximity to each other, making it difficult to distinguish the GMs from each other due to GM's artifacts, and causing that a small error in GM localization results in a big registration error. Additionally, the CT scan was acquired more than six weeks before the GBT procedure. As the patient received concurrent chemoradiation, the cervix and tumor sizes and positions are not accurate anymore. Lastly, CT has fewer soft tissue details, making it hard to distinguish the cervix from the tumor, probably resulting in inaccurate segmentation.

Even though the tumor tracking principle was not tested, as the GMs were not visible due to the applicator's artifacts, one single GM could be localized after insertion of the applicator, in procedure 1. This GM enabled the calculation of an additional translation of almost 3 cm, which was attributed to the pressure of the applicator on the cervix. Registration between the tips of Cath_{EM} and the tips of Cath_{MRI} showed that the inter-catheter geometry was alike, with an average error of 3.4 mm. Besides the earlier mentioned inaccuracy factors, this error could also be caused by inaccurate localization of the catheter tips in the postoperative MRI, which had a slice thickness of 3 mm, or by migration of the catheters inside the tissue in the time between insertion and scanning. Figure 32 shows that the uterus overlay of the transformed CT to postoperative MRI, based on catheter registration, is accurate. The distance between the CT uterus top and the postoperative MRI uterus top distance was 1.4 mm, which is a very low error for soft tissue registrations. The reconstructed catheters seem to be positioned at the same position in the cervix, but this is hard to quantify as it looks like the cervix was over-segmented in the CT, so the closest distance from the catheter to the cervix border gives misleading results.

Clinical relevance and scientific contribution
To the best of our knowledge, this was the first feasibility study to investigate the clinical workflow for EM-tracked GBT catheter insertion. Earlier studies researched the use of EM tracking for BT for other purposes, such as geometric assessment of placed catheters, applicator reconstruction, patient-individual quality assurance, or adaptive treatment planning [22, 38, 54]. Other studies described accurate real-time needle tracking workflows for GBT but used phantoms for testing and did not describe the image registration process in a clinical setting [21, 49, 52].

Another investigated approach for more accurate GBT freehand catheter insertion is applying generic or tailored 3D printed templates to the applicator to enhance the precision and simplicity of interstitial catheter placement [55–57]. However, one significant limitation of such a 3D-printed approach is the necessity of designing a new template for each patient, being time-consuming. Besides, the 3D printed material must be biocompatible, nontoxic, able to withstand sterilization, and should not affect the dose distributions, entailing substantial costs.

Freehand GBT catheter insertion requires technical skill and image guidance proficiency. Therefore, the insertion of a freehand catheter can be challenging and time-consuming. The therapeutic index of GBT is strongly depending on the quality of catheter implantation [5]. Underdosage of radiation to the tumor or excessive toxicity to organs at risk may occur due to inappropriate positioning of the catheters and sources [58]. Defining a clinically acceptable EM navigation error and catheter placement error is challenging due to limited information on current catheter placement accuracy. However, the current procedure relies on translating the preoperative 2D MRI slices to the 3D intraoperative situation, where soft tissue deformations occur, making it an inaccurate process. In our institution, situations occurred where the catheters were placed inaccurately, wherefore replacement of the

catheters, or adjustment of the dose planning was needed. The use of EM navigation for catheter insertion might therefore be beneficial and result in better accuracy in a shorter time. Besides, the learning curve for EM-navigated catheter insertion is steeper than the conventional workflow, as the navigation interface is intuitive and straightforward. However, it must also be noted that the entire GBT workflow is complex and requires significant coordination and cooperation of multiple departments (OR, radiology, radiotherapy) [6]. Adding navigation to the workflow will increase its complexity, necessitating technical expertise and close collaboration.

The relatively low number of complex GBT catheter insertion procedures, with only six patients per year in our institution, limits the widespread applicability and adoption of the EM navigation system. Besides, the information about the frequency of use of freehand catheters in other institutions is limited. However, especially because the complex GBT procedures are all unique and not one standard protocol or plan applies to the whole population, using EM navigation could be very helpful in improving the accuracy and efficiency of catheter placement during GBT procedures.

Besides, the potential for EM-tracked catheters extends beyond GBT. The workflow could also be used for interstitial prostate BT, where radioactive seeds are placed in a predefined location. The prostate is very well delineated with TRUS, making accurate registration and navigation feasible [21, 38]. The same EM tracking technology can be utilized in other applications, such as interventional radiology or minimally invasive procedures, where accurate catheter placement is crucial [18, 22]. However, these procedures require hollow catheters with the ability to aspirate or inject, requiring small adjustments to the needle [52].

Future directions
A prospective feasibility study is initiated at our institution to assess the feasibility of EM-navigation for gynecological brachytherapy catheter placement. Eligible study participants are 18 years and older and scheduled for 'complex' intrauterine BT catheter insertion. Exclusion criteria are metal implants in the pelvic or abdominal region and less than three gold anchors in the cervix at the time of the procedure. The study duration is one year, and a total of 6 patients (18 procedures) will be included. The study protocol was approved by the medical ethics committee in May 2023 (NL84035.041.23). The study starts when the first patient scheduled for complex BT catheter insertion is included. Appendix B describes a summary of the study protocol.

5 Conclusion

This study showed that EM navigation for gynecological brachytherapy catheter insertion is feasible in the research setting and has potential in the clinical setting. The proposed workflow has potential benefits that eliminate the need for intraoperative CBCT. This workflow can only truly be analyzed after the prospective clinical study in our institution.

6 Appendices

A Module explanation

Two 3D slicer modules were built specifically for the navigated brachytherapy catheter insertion procedure: Module ‘preparation’ for initializing US calibration in the 3D Slicer scene and module ‘Brachy_camera_set’ for controlling the point of view of the scene. The modules are written in Python language and by using a Graphical User Interface (GUI) designer.

Preparation
The module ‘preparation’ is written to initialize the scene to correctly read the ultrasound information in the slicer scene. For registration, we want to know the location of each pixel in the US image in millimeters, relative to the reference sensor. The important incoming information from the BK ultrasound device are the pixel values at specified locations [pixel], the pixel spacing [mm/pixel] and the US image origin [pixel]. The latter varies when adjusting the zoom. We use this information to specify the pixel locations in mm relative to the US image origin. As the location of the US sensor is known relative to the US image, calculated with the US calibration, we US pixel locations are known relative to the US sensor. Using this information, we know the location of the pixels in the EM-field.

With this module, three transformation matrices are specified and put in order:

- US calibration (axial or sagittal)
  - zoom
    - ImageToProbe

The zoom transformation matrix automatically changes when the zoom is adjusted on the BK device. Also when the view of the US probe is changed from axial to sagittal, the script automatically chooses the right calibration matrix.

One disadvantage of the used BK device was that we could only broadcast the total BK screen in 3D Slicer, instead of only the US pixels. This caused that adjustments of the BK device settings, such as image screen zoom (not to be confused with US zoom), were also visualized in 3D Slicer, influencing the transformation matrices while they actually should not.

Brachy_camera_set
This module was designed to optimize the user interface in 3D Slicer. In this module, the user can toggle between different views. Three different views follow the needle tip: two from behind the needle, of which one exactly in line (first person view) and one from above (third person view) and one from the side, perpendicular to the needle (side view). The last option is a global view, where the camera does not follow the needle. Experience has taught us that visualizing one ’needle following view’, and one ’global view’, works most effectively.

B Summary study protocol NL84035.041.23

Rationale: Image-guided navigation surgery allows for optimal use and full integration of 3D models based on patient-specific anatomy. Image-guided techniques have proven to be useful for the localization and visualization of lesions and might be of use for gynecological brachytherapy catheter placement, especially for freehand catheters. This is the first feasibility study where electromagnetic (EM)-tracking is used for real-time navigated gynecological brachytherapy (BT) catheter placement.
Objective: The primary objective of this study is to assess the feasibility of EM-navigation for gynecological brachytherapy catheter placement.
Study design: A single-center feasibility study.
Study population: Patients scheduled for intrauterine brachytherapy application with one or more freehand catheters additional to the catheters through the applicator. A total of 6 patients (18 procedures) will be included.
Intervention: Tumor registration is performed using the standard transrectal ultrasound transducer (standard care), using the placed GMs (standard care) as landmarks. A custom-developed stylet inside the standard freehand catheters is tracked and can thus be used to visualize the catheters in real-time relative to the 3D MRI model. The RTO uses cone beam CT when desired to validate brachytherapy catheter placement, as during the standard procedure.
Main study parameters/endpoints: The main study endpoint is the feasibility of image-guided navigation with EM-tracking for assistance during gynecologic brachytherapy catheter placement. Feasibility is defined as successful when 80% of the navigations are successful. Navigation is successful when the fiducial root mean square error (RMSE) for gold marker MRI to US registration is below 5 mm.
Nature and extent of the burden and risks associated with participation, benefit, and group relatedness: Participation in the study will not involve additional visits to the hospital for the included patients. Patients will be informed about the study during the pre-operative outpatient clinic appointment. Informed consent will be obtained during one of the patient's visits to the hospital. Catheter placement takes place with conventional decision-making, by using ultrasound and cone beam CT. The RTOs are aware of the experimental setup and are therefore responsible for the navigation interpretation and actions. During the procedure, the accuracy of the registration is assessed by checking the overlap of MRI and ultrasound anatomy (bladder, cervix, etc.). The ultimate goal of this project is to judge the potential use of the navigation setup for further gynecological BT catheter placement procedures. A maximal delay of 15 minutes will be added to the total time of the surgical procedure.

Bibliography

[1] H. Ellis, "Anatomy of the uterus," *Anaesthesia Intensive Care Medicine*, vol. 12, pp. 99–101, 3 2011.

[2] A. M. R. Agur and A. F. Dalley, *Grant's Atlas of Anatomy (13th Ed)(gnv64).pdf*, 2013.

[3] A. Taylor and M. E. Powell, "An assessment of interfractional uterine and cervical motion: Implications for radiotherapy target volume definition in gynaecological cancer," *Radiotherapy and Oncology*, vol. 88, pp. 250–257, 8 2008.

[4] B. Chaurasia, *BD Chaurasia's Human Anatomy, Volume 2: Regional and Applied Dissection and Clinical: Lower Limb, Abdomen and Pelvis*. CBS Publishers & Distributors, 2019. [Online]. Available: https://books.google.nl/books?id=PaQSyAEACAAJ

[5] C. Chargari, E. Deutsch, P. Blanchard, S. Gouy, H. Martelli, F. Guérin, I. Dumas, A. Bossi, P. Morice, A. N. Viswanathan, and C. Haie-Meder, "Brachytherapy: An overview for clinicians," *CA: A Cancer Journal for Clinicians*, vol. 69, pp. 386–401, 9 2019. [Online]. Available: https://onlinelibrary.wiley.com/doi/full/10.3322/caac.21578https://onlinelibrary.wiley.com/doi/abs/10.3322/caac.21578https://acsjournals.onlinelibrary.wiley.com/doi/10.3322/caac.21578

[6] J. I. Prisciandaro, X. Zhao, S. Dieterich, Y. Hasan, S. Jolly, and H. A. Al-Hallaq, "Interstitial high-dose-rate gynecologic brachytherapy: Clinical workflow experience from three academic institutions," *Seminars in Radiation Oncology*, vol. 30, pp. 29–38, 1 2020.

[7] R. A. Nout, V. T. Smit, H. Putter, I. M. Jürgenliemk-Schulz, J. J. Jobsen, L. C. Lutgens, E. M. van der Steen-Banasik, J. W. Mens, A. Slot, M. S. Kroese, B. N. van Bunningen, A. C. Ansink, W. L. van Putten, and C. L. Creutzberg, "Vaginal brachytherapy versus pelvic external beam radiotherapy for patients with endometrial cancer of high-intermediate risk (portec-2): an open-label, non-inferiority, randomised trial," *The Lancet*, vol. 375, pp. 816–823, 3 2010.

[8] K. Albuquerque, B. A. Hrycushko, M. M. Harkenrider, J. Mayadev, A. Klopp, S. Beriwal, D. G. Petereit, D. J. Scanderbeg, and C. Yashar, "Compendium of fractionation choices for gynecologic hdr brachytherapy—an american brachytherapy society task group report," *Brachytherapy*, vol. 18, pp. 429–436, 7 2019.

[9] T. P. Hellebust, C. Kirisits, D. Berger, J. Pérez-Calatayud, M. D. Brabandere, A. D. Leeuw, I. Dumas, R. Hudej, G. Lowe, R. Wills, and K. Tanderup, "Recommendations from gynaecological (gyn) gec-estro working group: Considerations and pitfalls in commissioning and applicator reconstruction in 3d image-based treatment planning of cervix cancer brachytherapy," *Radiotherapy and Oncology*, vol. 96, pp. 153–160, 8 2010.

[10] Venezia | brachytherapy | gynecological applicator | elekta. [Online]. Available: https://www.elekta.com/products/brachytherapy/venezia/

[11] P. Gavriilidis, B. Edwin, E. Pelanis, E. Hidalgo, N. de'Angelis, R. Memeo, L. Aldrighetti, and R. P. Sutcliffe, "Navigated liver surgery: State of the art and future perspectives," *Hepatobiliary Pancreatic Diseases International*, vol. 21, pp. 226–233, 6 2022.

[12] E. N. Kok, R. Eppenga, K. F. Kuhlmann, H. C. Groen, R. van Veen, J. M. van Dieren, T. R. de Wijkerslooth, M. van Leerdam, D. M. Lambregts, W. J. Heerink, N. J. Hoetjes, O. Ivashchenko, G. L. Beets, A. G. Aalbers, J. Nijkamp, and T. J. Ruers, "Accurate surgical navigation with real-time tumor tracking in cancer surgery," *npj Precision Oncology 2020 4:1*, vol. 4, pp. 1–7, 4 2020. [Online]. Available: https://www.nature.com/articles/s41698-020-0115-0

[13] T. Langø, G. A. Tangen, R. Mårvik, B. Ystgaard, Y. Yavuz, J. H. Kaspersen, O. V. Solberg, and T. A. Hernes, "Navigation in laparoscopy – prototype research platform for improved image-guided surgery," *http://dx.doi.org/10.1080/13645700701797879*, vol. 17, pp. 17–33, 2009. [Online]. Available: https://www.tandfonline.com/doi/abs/10.1080/13645700701797879

[14] J. Nijkamp, K. F. Kuhlmann, O. Ivashchenko, B. Pouw, N. Hoetjes, M. A. Lindenberg, A. G. Aalbers, G. L. Beets, F. van Coevorden, N. KoK, and T. J. Ruers, "Prospective study on image-guided navigation surgery for pelvic malignancies," *Journal of Surgical Oncology*, vol. 119, pp. 510–517, 3 2019. [Online]. Available: https://onlinelibrary.wiley.com/doi/full/10.1002/jso.25351https://onlinelibrary.wiley.com/doi/abs/10.1002/jso.25351https://onlinelibrary.wiley.com/doi/10.1002/jso.25351

[15] P. Waelkens, M. N. van Oosterom, N. S. van den Berg, N. Navab, and F. W. B. van Leeuwen, "Surgical navigation: An overview of the state-of-the-art clinical applications," *Radioguided Surgery*, pp. 57–73, 2016. [Online]. Available: https://link.springer.com/chapter/10.1007/978-3-319-26051-8_4

[16] F. Attivissimo, A. M. L. Lanzolla, S. Carlone, P. Larizza, and G. Brunetti, "A novel electromagnetic tracking system for surgery navigation," *https://doi.org/10.1080/24699322.2018.1529199*, vol. 23, pp. 42–52, 1 2018. [Online]. Available: https://www.tandfonline.com/doi/abs/10.1080/24699322.2018.1529199

[17] "Aurora sensors - ndi." [Online]. Available: https://www.ndigital.com/electromagnetic-tracking-technology/aurora/aurora-sensors/

[18] A. M. Franz, T. Haidegger, W. Birkfellner, K. Cleary, T. M. Peters, and L. Maier-Hein, "Electromagnetic tracking in medicine -a review of technology, validation, and applications," *IEEE Transactions on Medical Imaging*, vol. 33, pp. 1702–1725, 2014.

[19] A. Sorriento, M. B. Porfido, S. Mazzoleni, G. Calvosa, M. Tenucci, G. Ciuti, and P. Dario, "Optical and electromagnetic tracking systems for biomedical applications: A critical review on potentialities and limitations," *IEEE Reviews in Biomedical Engineering*, vol. 13, pp. 212–232, 2020.

[20] "E30 case report image fusion and electromagnetic needle tracking for the biopsy of pelvic lesions-report of 2 cases."

[21] L. Beaulieu, E. Racine, D. Y. Han, E. Vigneault, I. C. Hsu, and J. A. M. Cunha, "Real-time electromagnetic tracking–based treatment platform for high-dose-rate prostate brachytherapy: Clinical workflows and end-to-end validation," *Brachytherapy*, vol. 17, pp. 103–110, 1 2018.

[22] N. N. Janssen, H. Brastianos, A. Akingbade, T. Olding, T. Vaughan, T. Ungi, A. Lasso, C. Joshi, M. Korzeniowski, C. Falkson, and G. Fichtinger, "Electromagnetic (em) catheter path tracking in ultrasound-guided brachytherapy of the breast," *International journal of computer assisted radiology and surgery*, vol. 15, pp. 1645–1652, 10 2020. [Online]. Available: https://pubmed.ncbi.nlm.nih.gov/32712885/

[23] S. H. Kim, S. J. Lee, M. H. Choi, H. J. Yang, J. E. Kim, K. H. Huh, S. S. Lee, M. S. Heo, S. J. Hwang, and W. J. Yi, "Quantitative augmented reality-assisted free-hand orthognathic surgery using electromagnetic tracking and skin-attached dynamic reference," *The Journal of craniofacial surgery*, vol. 31, pp. 2175–2181, 11 2020. [Online]. Available: https://journals.lww.com/jcraniofacialsurgery/Fulltext/2020/12000/Quantitative_Augmented_Reality_Assisted_Free_Hand.17.aspx

[24] F. Heijden, "Snt 1 – point registration," *Syllabus Technical Medicine, University of Twente*, vol. 1, no. 1, pp. 1–27, 8 2020.

[25] L. Li, R. Wang, and X. Zhang, "A tutorial review on point cloud registrations: Principle, classification, comparison, and technology challenges," *Mathematical Problems in Engineering*, vol. 2021, 2021.

[26] J. M. Fitzpatrick, "Fiducial point placement and the accuracy of point-based, rigid body registration," 2001. [Online]. Available: https://www.researchgate.net/publication/12014587

[27] J. A. Jensen, "Medical ultrasound imaging," *Progress in Biophysics and Molecular Biology*, vol. 93, pp. 153–165, 1 2007.

[28] L. E. Bø, E. F. Hofstad, F. Lindseth, and T. A. Hernes, "Versatile robotic probe calibration for position tracking in ultrasound imaging," *Physics in Medicine Biology*, vol. 60, p. 3499, 4 2015. [Online]. Available: https://iopscience.iop.org/article/10.1088/0031-9155/60/9/3499https://iopscience.iop.org/article/10.1088/0031-9155/60/9/3499/meta

[29] C. Gsaxner, A. Pepe, J. Li, U. Ibrahimpasic, J. Wallner, D. Schmalstieg, and J. Egger, "Augmented reality for head and neck carcinoma imaging: Description and feasibility of an instant calibration, markerless approach," *Computer Methods and Programs in Biomedicine*, vol. 200, p. 105854, 2021. [Online]. Available: www.elsevier.com/locate/cmpb

[30] T. Yang, S. Lin, Q. Xie, W. Ouyang, T. Tan, J. Li, Z. Chen, J. Yang, H. Wu, J. Pan, C. Hu, and Y. Zou, "Impact of 3d printing technology on the comprehension of surgical liver anatomy abbreviations 2d two-dimensional 3d three-dimensional 3dp three-dimensional printing ct computed tomography mdct multi-detector computed tomography vir three-dimensional virtual reconstruction and other interventional techniques," *Surgical Endoscopy*, vol. 33, pp. 411–417, 2019. [Online]. Available: https://doi.org/10.1007/s00464-018-6308-8

[31] H. Choi, B. Cho, K. Masamune, M. Hashizume, and J. Hong, "An effective visualization technique for depth perception in augmented reality-based surgical navigation," *The International Journal of Medical Robotics and Computer Assisted Surgery*, vol. 12, pp. 62–72, 3 2016. [Online]. Available: https://onlinelibrary.wiley.com/doi/full/10.1002/rcs.1657https://onlinelibrary.wiley.com/doi/abs/10.1002/rcs.1657https://onlinelibrary.wiley.com/doi/10.1002/rcs.1657

[32] F. M. Sánchez-Margallo, J. A. Sánchez-Margallo, J. L. Moyano-Cuevas, E. M. Pérez, J. Maestre, F. M. S. anchez Margallo, J. A. S. anchez Margallo, J. L. Moyano-Cuevas, and E. P. M. ıa erez, "Use of natural user interfaces for image navigation during laparoscopic surgery: initial experience," *http://dx.doi.org/10.1080/13645706.2017.1304964*, vol. 26, pp. 253–261, 9 2017. [Online]. Available: https://www.tandfonline.com/doi/abs/10.1080/13645706.2017.1304964

[33] "Verordening (eu) 2017/ 745 van het europees parlement en de raad - van 5 april 2017 - betreffende medische hulpmiddelen, tot wijziging van richtlijn 2001/ 83/ eg, verordening (eg) nr. 178/ 2002 en verordening (eg) nr. 1223/ 2009, en tot intrekking van richtlijnen 90/ 385/ eeg en 93/ 42/ eeg van de raad."

[34] "Richtlijn beoordelingscriteria herbruikbare medische hulpmiddelen - vdsmh." [Online]. Available: https://www.vdsmh.nl/publicaties/algemeen/richtlijn-beoordelingscriteria-herbruikbare-medische-hulpmiddelen

[35] K. Grewal, B. Jones, A. L'Heveder, S. Jindal, N. Galazis, S. Saso, and J. Yazbek, "The use of intra-operative ultrasound in gynecological surgery: a review," *Future Science OA*, vol. 7, 3 2021.

[36] C. A. Woodfield, "The usefulness of ultrasound imaging in gynecologic oncology," *PET Clinics*, vol. 13, pp. 143–163, 4 2018.

[37] E. C. Fields, S. Hazell, M. Morcos, E. J. Schmidt, C. Chargari, and A. N. Viswanathan, "Image-guided gynecologic brachytherapy for cervical cancer," *Seminars in Radiation Oncology*, vol. 30, pp. 16–28, 1 2020.

[38] S. Bharat, C. Kung, E. Dehghan, A. Ravi, N. Venugopal, A. Bonillas, D. Stanton, and J. Kruecker, "Electromagnetic tracking for catheter reconstruction in ultrasound-guided high-dose-rate brachytherapy of the prostate," *Brachytherapy*, vol. 13, pp. 640–650, 11 2014. [Online]. Available: http://www.brachyjournal.com/article/S153847211400539X/fulltexthttp://www.brachyjournal.com/article/S153847211400539X/abstracthttps://www.brachyjournal.com/article/S1538-4721(14)00539-X/abstract

[39] R. P. van den Ende, L. S. Rigter, E. M. Kerkhof, E. L. van Persijn van Meerten, E. C. Rijkmans, D. M. Lambregts, B. van Triest, M. E. van Leerdam, M. Staring, C. A. Marijnen, and U. A. van der Heide, "Mri visibility of gold fiducial markers for image-guided radiotherapy of rectal cancer," *Radiotherapy and Oncology*, vol. 132, pp. 93–99, 3 2019. [Online]. Available: http://www.thegreenjournal.com/article/S0167814018336090/fulltexthttp://www.thegreenjournal.com/article/S0167814018336090/abstracthttps://www.thegreenjournal.com/article/S0167-8140(18)33609-0/abstract

[40] uhu. Uhu plus schnellfest two-component adhesive 45700 35 g | conrad.com. [Online]. Available: https://www.conrad.com/p/uhu-plus-schnellfest-two-component-adhesive-45700-35-g-478703

[41] A. Fedorov, R. Beichel, J. Kalpathy-Cramer, J. Finet, J. C. Fillion-Robin, S. Pujol, C. Bauer, D. Jennings, F. Fennessy, M. Sonka, J. Buatti, S. Aylward, J. V. Miller, S. Pieper, and R. Kikinis, "3d slicer as an image computing platform for the quantitative imaging network," *Magnetic Resonance Imaging*, vol. 30, pp. 1323–1341, 11 2012.

[42] A. Lasso, T. Heffter, A. Rankin, C. Pinter, T. Ungi, and G. Fichtinger, "Plus: Open-source toolkit for ultrasound-guided intervention systems," *IEEE Transactions on Biomedical Engineering*, vol. 61, pp. 2527–2537, 10 2014.

[43] T. Ungi, A. Lasso, and G. Fichtinger, "Open-source platforms for navigated image-guided interventions," *Medical image analysis*, vol. 33, pp. 181–186, 10 2016. [Online]. Available: https://pubmed.ncbi.nlm.nih.gov/27344106/

[44] A great fiducial marker that helps improve radiotherapy • gold anchor. [Online]. Available: https://www.goldanchormarker.com/

[45] Visicoil fiducial marker — izi medical. [Online]. Available: https://izimed.com/visicoil-fiducial-marker

[46] O. Tanaka, T. Iida, H. Komeda, M. Tamaki, K. Seike, D. Kato, T. Yokoyama, S. Hirose, and D. Kawaguchi, "Initial experience of using an iron-containing fiducial marker for radiotherapy of prostate cancer: Advantages in the visualization of markers in computed tomography and magnetic resonance imaging," *Polish Journal of Medical Physics and Engineering*, vol. 22, pp. 93–96, 12 2016.

[47] M. F. Chan, G. N. Cohen, and J. O. Deasy, "Qualitative evaluation of fiducial markers for radiotherapy imaging," *Technology in cancer research treatment*, vol. 14, pp. 298–304, 6 2015. [Online]. Available: https://pubmed.ncbi.nlm.nih.gov/25230715/

[48] J. Hummel, M. Figl, W. Birkfellner, M. R. Bax, R. Shahidi, C. R. Maurer, and H. Bergmann, "Evaluation of a new electromagnetic tracking system using a standardized assessment protocol," *Physics in Medicine and Biology*, vol. 51, 5 2006.

[49] S. Boutaleb, E. Racine, O. Fillion, A. Bonillas, G. Hautvast, D. Binnekamp, and L. Beaulieu, "Performance and suitability assessment of a real-time 3d electromagnetic needle tracking system for interstitial brachytherapy," *Journal of Contemporary Brachytherapy*, vol. 7, pp. 280–289, 2015.

[50] E. Poulin, E. Racine, D. Binnekamp, and L. Beaulieu, "Fast, automatic, and accurate catheter reconstruction in hdr brachytherapy using an electromagnetic 3d tracking system," *Medical physics*, vol. 42, pp. 1227–1232, 3 2015. [Online]. Available: https://pubmed.ncbi.nlm.nih.gov/25735278/

[51] G. Pu, S. Jiang, Z. Yang, Y. Hu, and Z. Liu, "A novel ultrasound probe calibration method for multimodal image guidance of needle placement in cervical cancer brachytherapy," *Physica Medica*, vol. 100, pp. 81–89, 8 2022.

[52] A. Mehrtash, "Needle navigation for image guided brachytherapy of gynecologic," 2020. [Online]. Available: http://www.kth.se/sth

[53] D. Batchelar, M. Gaztañaga, M. Schmid, C. Araujo, F. Bachand, and J. Crook, "Validation study of ultrasound-based high-dose-rate prostate brachytherapy planning compared with ct-based planning," *Brachytherapy*, vol. 13, pp. 75–79, 1 2014.

[54] B. C. Sauer, C. Dürrbeck, and C. Bert, "Electromagnetic tracking in interstitial brachytherapy: A systematic review," *Frontiers in Physics*, vol. 10, p. 956983, 9 2022.

[55] M. Marar, E. Simiele, T. Niedermayr, and E. A. Kidd, "Applying 3d-printed templates in high-dose-rate brachytherapy for cervix cancer: Simplified needle insertion for

optimized dosimetry," *International Journal of Radiation Oncology*Biology*Physics*, vol. 114, pp. 111–119, 9 2022.

[56] J. J. Sohn, M. Polizzi, D. Richeson, S. Gholami, I. J. Das, and W. Y. Song, "A novel workflow with a customizable 3d printed vaginal template and a direction modulated brachytherapy (dmbt) tandem applicator for adaptive interstitial brachytherapy of the cervix," *Journal of Clinical Medicine 2022, Vol. 11, Page 6989*, vol. 11, p. 6989, 11 2022. [Online]. Available: https://www.mdpi.com/2077-0383/11/23/6989/htmhttps://www.mdpi.com/2077-0383/11/23/6989

[57] L. Zwetsloot, "The future of interstitial brachytherapy : development of a 3d printed add-on for improved needle placement in interstitial brachytherapy for patients with paravaginal tumors," September 2022. [Online]. Available: http://essay.utwente.nl/92872/

[58] K. Majercakova, R. Pötter, C. Kirisits, S. Banerjee, A. E. Sturdza, P. Georg, N. Nesvacil, and M. P. Schmid, "Evaluation of planning aims and dose prescription in image-guided adaptive brachytherapy and radiochemotherapy for cervical cancer: Vienna clinical experience in 225 patients from 1998 to 2008," *http://dx.doi.org/10.3109/0284186X.2015.1063783*, vol. 54, pp. 1551–1557, 10 2015. [Online]. Available: https://www.tandfonline.com/doi/abs/10.3109/0284186X.2015.1063783